Matched field beamforming applied to sonar data

TOMAS LUNDSTRÖM

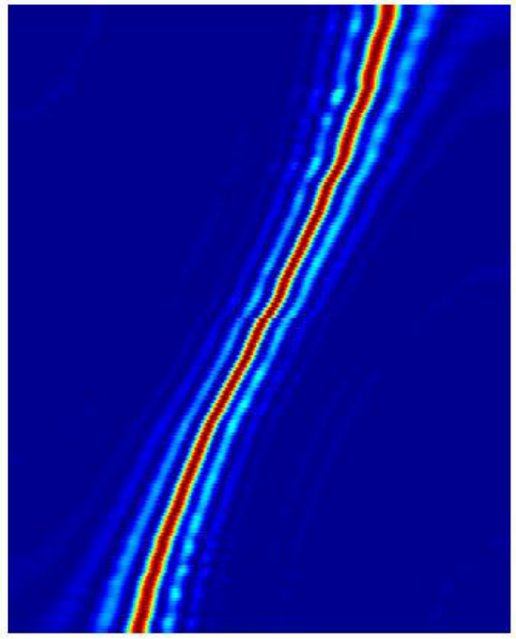

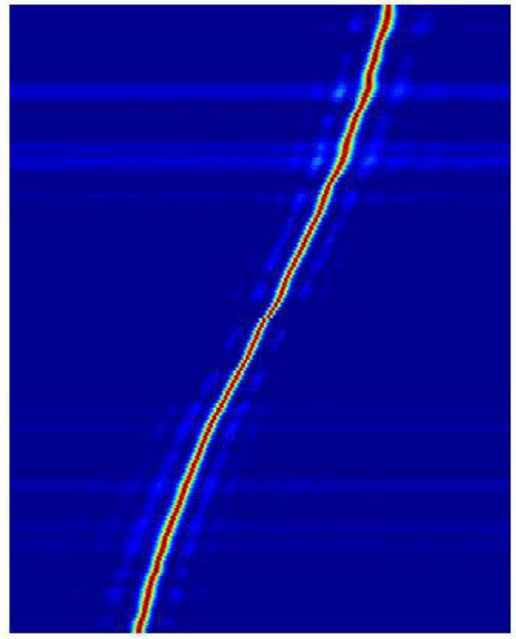

FOI
Defence Research Agency
Defence & Security, Systems and Technology
SE-164 90 Stockholm

Phone: +46 8 555 030 00
Fax: +46 8 555 031 00

www.foi.se

FOI-R--2731--SE
ISSN 1650-1942

Technical report
March 2009

Defence & Security, Systems and Technology

Tomas Lundström

Matched field beamforming applied to sonar data

Titel	Anpassad lobformning för sonardata
Title	Matched field beamforming applied to sonar data

Rapportnr/Report no	FOI-R--2731--SE
Rapporttyp Report Type	Teknisk rapport Technical report
Sidor/Pages	67 p
Månad/Month	Mars/March
Utgivningsår/Year	2009
ISSN	ISSN 1650-1942
Kund/Customer	FMV
Forskningsområde Programme area	4. Sensorer och signaturanpassning 4. Sensors and Low Observables
Delområde Subcategory	43 UV-teknik – sensorer 43 Underwater Technology - Surveillance, Target acquisition and Reconnaissance
Projektnr/Project no	E28118
Godkänd av/Approved by	Helena Bergman

FOI, Totalförsvarets Forskningsinstitut	FOI, Swedish Defence Research Agency
Avdelningen för Försvars- och säkerhetssystem	Defence & Security, Systems and Technology
164 90 Stockholm	SE-164 90 Stockholm

Sammanfattning

Två metoder är utvecklade och utvärderade för att förbättra lobformning. Metoderna estimerar utseendet av vågfronten och använder den informationen för att förbättra lobformningen. En av metoderna använder uppskattningar av tidsskillnader mellan sensorerna för att approximera utseendet av vågfronten, och den andra approximerar vågfronten genom att matcha den mottagna vågfronten mot sfäriska vågfronter med olika krökningsradier. Metoderna är jämförda med en tredje metod, som antar att inkommande våg är plan. Metodernas avståndsuppskattning är också utvärderade.

Båda metoderna testades med verkliga och simulerade data. Simulerade data erhölls ifrån Raylab, vilket är ett simuleringsprogram som använder strålgångs metodik. De verkliga data kom från ett fältförsök i Östersjön med en släpsonar där en stillaliggande källa sände ut toner.

Förbättringarna hos de utvecklade metoderna beror på avståndet till målet. Vid ett avstånd av 600 m framför antennerna ökar den mottagna effekten med 0.5-1 dB jämfört med planvågslobforming. Vid ett avstånd av 300 m framför antennerna ökar den mottagna effekten med cirka 2 dB. Det visade sig att det är svårt att uppskatta avståndet till målet och estimeringen är beroende av bruset i miljön. Ett mål under rörelse, vid ett avstånd av 600 m, kan avståndsbestämmas med ett fel på 150 m, när rekursiv uppdatering av kovariansmatrisen med en uppdateringskonstant på 0.25 används. När rekursiv uppdatering inte används ökar felet till 400 m.

Nyckelord: Konventionell lobformning, Närfält, Bäringsestimering, Avstånds-uppskattning, Sonar, MUSIC, Linjär antenn, Spatial kovariansmatris, Matchat fält

Summary

Two methods for evaluating and improving wave beamforming have been developed. The methods estimate the shape of the wavefront and use the information in the beamforming. One of the methods uses estimates of the time delays between the sensors to approximate the shape of the wavefront, and the other estimates the wavefront by matching the received wavefront to spherical wavefronts of different radii. The methods are compared to a third more common method of beamforming, which assumes that the impinging wave is planar. The passive ranging abilities of the methods are also evaluated, and compared to a reference method based on triangulation.

Both methods were evaluated with both real and simulated data. The simulated data was obtained using Raylab, which is a simulation program based on ray tracing. The real data was obtained through a field-test performed in the Baltic Sea using a towed array sonar and emitted tones from a stationary source.

The performance of the matched beamformers depends on the distance to the target. At a distance of 600 m near broadside the power received by the beamformer increases by 0.5-1 dB compared to the plane wave beamformer. At a distance of 300 m near broadside the improvement is approximately 2 dB. In general, obtaining an accurate distance estimation proved to be difficult, and highly dependent on the noise present in the environment. A moving target at a distance of 600 m at broadside can be estimated with a maximum error of 150 m, when recursive updating of the covariance matrix with an updating constant of 0.25 is used. When recursive updating is not used the margin of error increases to 400 m.

Keywords: Conventional beamforming, Nearfield, Bearing estimation, Distance estimation, Sonar, MUSIC, Linear array, Spatial covariance matrix, Matched field

Contents

1 Acknowledgments

I would like to thank all the people at FOI for their support during the time at FOI and for a great master thesis experience. I especially would like to thank my supervisors Leif Persson, Alex Cederholm and Jörgen Phil for always taking the time to answer my questions and giving me good advice. I would also like to thank my examiner Fredrik Gustafsson, university supervisor Martin Skoglund and my scientific reviewer Ilkka Karasalo at FOI for showing interest in my work and giving useful comments. Also thanks to Carl Gerhardsson (FMV) and Viktoria Zetterberg (FMV) for funding this project.

Finally I would like to thank my girlfriend Ashley for all the help and support during my thesis.

2 Abbreviations and symbols

Bias	deviation from true value
Broadside angle	The impinging angle when the source is located perpendicular to the linear array
BTR	Bearing Time Record
CB	Conventional Beamforming
CPA	Closest Point of Approach
DOA	Direction Of Arrival
Endfire angle	The impinging angle when the source is located on the same line as the linear array
FFT	Fast Fourier Transform
MUSIC	Multiple Signal Classification
SAS	Synthetic Aperture Sonar
SCM	Spatial Covariance Matrix
SNR	Signal to Noise Ratio
SONAR	Sound Navigation and Ranging
TAS	Towed Array Sonar

3 Introduction

Sonar [1] *is a system that uses the acoustical waves in water for detection of objects. Animals have been doing this naturally for millions of years and the first human to use sound for detection of objects was Leonardo Da Vinci in 1490. Sonar is especially useful for characterizing and navigating in marine environments. This feature is of importance to navies around the world as they defend their coastal borders, for example from divers, submarines and fast moving surface vehicles [15]. Sonar systems are becoming increasingly sophisticated especially the software components. The development is costly and the models and methods have to be thoroughly tested and evaluated.*

3.1 Background

Sonar uses hydrophones, which are electro acoustic transducers used specifically for underwater applications, to convert sound signals into electrical signals [4]. There are two types of sonar systems, *active* and *passive* sonar, the latter is used in this thesis.

Active sonar systems transmit sound waves and then listen for reflections of the pulse. The distance to a given object can be measured by converting the pulse transmission time according to the speed of sound in the environment. The bearing to a given target can be measured using an array of hydrophones and the various arrival times of the wave fronts. This procedure is termed echo-ranging, and with sophisticated signal processing, directional sources and multiple receivers highly accurate estimations can be achieved.

Passive sonar systems only listen for acoustic waves, they do not transmit waves. The received signal is often degraded due to underwater propagation effects, ambient noise and interfering signal sources such as surface ships, marine animals, sea life and ice. Noise can also be produced from the platform carrying the sonar. Passive sonar is mostly used for military purposes with one of the most important applications being ship and submarine detection. At high noise levels performance is reduced, however by using appropriate signal processing techniques useful data can still be obtained.

Beamforming is a signal processing technique that originates from the design of spatial filters with pencil shaped directional sensitivity to strengthen signals in a specified direction and attenuate signals from other directions. Implementing spatial filters requires sampled data from various spatial locations. The processor that performs the filtering is called $beamformer$ [4].

There are various types of hydrophone assemblies, such as Flank Array Sonar (FAS) and Towed Array Sonar (TAS)[9]. The experimental data used in this thesis was obtained from a TAS. A TAS is a long flexible hose attached to a surface ship or a submarine through a connecting cable, see Figure 3.1.

The hose has a large number of hydrophones attached to it, and by processing the signal as in Section 4.3 the bearing of the target can be estimated.

Advantages of using a TAS are:

- The aperture of the array can be made very long, because the size of

[1] SOund NAvigation and Ranging

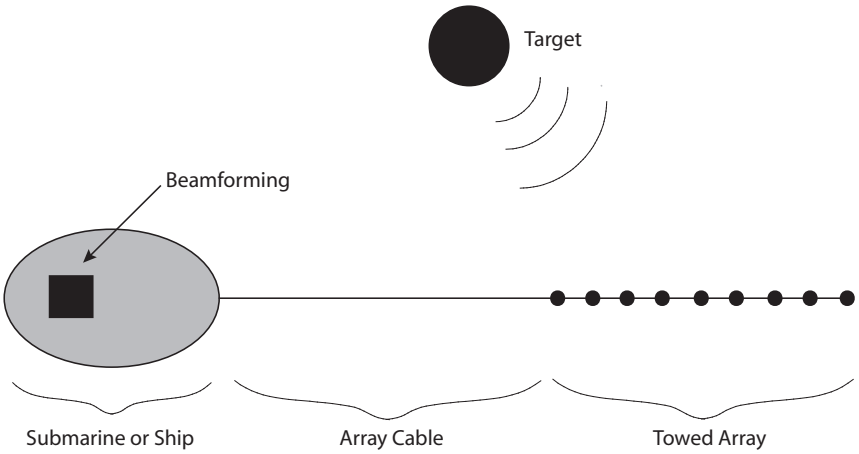

Figure 3.1: A TAS connected to a vessel.

the array is not limited by the size of the ship or the submarine. The resolution of the array is inversely proportional to the length of the array, hence a longer array gives a higher resolution.

- The TAS can be towed at a depth where the propagation of sound is optimal while the submarine travels at another depth, ideally one at which sound propagation is diminished, enabling it to avoid detection.

- Having a long cable between the hydrophones and the vessel reduces the self noise from the vessel.

3.2 Problem statement

Target detection is the primary application of sonar systems. The ability to detect a target depends on the processing method. If the target is located in the near field of the antenna the beamformer will suffer a severe degradation if the curvature of the wavefront is not compensated for.

The main objective of this master thesis is to determine to which degree the beamforming can be improved by adjusting the beamforming algorithm to the received wavefront. Key problems and possible solutions will be explored and discussed. The main challenges and how can they be solved or the effects of them be minimized will be addressed.

The goal is to show that there are advantages when using a beamformer which uses information about the wavefront. All results will be explained theoretically, supported by simulations and tested using experimental data from a field test. The methods will be compared to a plane wave beamformer.

3.3 Related work

The majority of the literature about beamforming focuses on far field detection. In order to estimate the curvature of the wavefront, time delays between

elements have to be estimated. In [5] a way to process the signal to achieve optimum bearing and distance estimates is discussed using time delay estimates. The processing of the signal assumes that the exact power spectrum for the signal and the noise is known for every sensor and that there is no multipath present. In [11] passive range estimation is discussed. New developments in TAS research are discussed in [9]. [16] discusses near field beamforming for microphone antennas within room acoustics.

3.4 Approach

The following steps are taken to answer the problems stated in Section 3.2:

1. Implement algorithms.
2. Test and evaluate algorithms using simulated data.
3. Test and evaluate algorithms using experimental data.
4. Solve and minimize the effects of the discovered problems and verify with simulations.

3.5 Data model

In this thesis the signals from the sources are assumed to be narrow band signals, which can be expressed as

$$s(t) = a(t)\sin(2\pi f t + \phi(t))\,, \tag{3.1}$$

where f is the frequency of the source, ϕ is the phase of the signal, t is the time and $a(t)$ is the amplitude of the signal. The signal received at the mth sensor is expressed as

$$x_m(t) = \sum_{n=1}^{N} h_m(t) * s_n(t - \tau_{mn}(\phi)) + v_m(t)\,, \tag{3.2}$$

where $h_m(t)$ is the impulse response of the mth sensor, $\{s_n(t)\}_{n=1}^{N}$ are the radiated signals from the sources, $\{v_m(t)\}_{m=1}^{N}$ are additive noise processes and τ_{mn} are delays associated with the propagation time across the array. The sensors are assumed to be omni directional and identical with impulse responses $h_m(t) = \delta(t)$. For the case of a single source (3.2) reduces to

$$x_m(t) = s(t - \tau_m(\phi)) + v_m(t)\,. \tag{3.3}$$

From τ_m information about the source distance to the array can be extracted by calculating the curvature of the wavefront.

3.6 Thesis outline

Chapter 4 gives an introduction to linear arrays and beamforming in general, followed by a part that discusses two methods for wavefront estimation. In Chapter 5 the data used to analyze the different methods are introduced, the first part discusses the data from a field test followed by a part about the simulated data. The results are presented in Chapter 6. This is followed by conclusions in Chapter 7.

4 Methods

4.1 Linear array

To determine bearing to a source, often an array of sensors is used. The sensors can be arranged in various ways, for example a circular array, where N sensors are positioned in a circle. In this thesis a linear array of sensors will be addressed. When choosing the distance between the elements in the array care has to be taken because the propagating wavefield can be undersampled which leads to spatial aliasing. This is shown as one or more focus points in the power bearing diagram, called grating lobes. The limit for avoiding spatial aliasing is set by the distance between the elements. If the distance exceeds that limit, grating lobes will appear which affects the bearing estimation in a negative way. To avoid grating lobes the distance between two adjacent elements has to satisfy

$$d \leq \lambda/2\,, \tag{4.1}$$

where d is the distance between the sensors in the array and λ is the wavelength [3],[10]. The beam pattern for a linear array is given by

$$B(\theta,\phi) = \sum_{m=1}^{N} w_m e^{j\frac{2\pi}{\lambda}(\sin\theta\cos\phi x_m + \sin\theta\sin\phi y_m + \cos\theta z_m)}\,, \tag{4.2}$$

where w_m are the weights of every sensor [14]. The parameters x_m, y_m, z_m are the Cartesian coordinates for the mth sensor, θ is the polar angle and ϕ is the azimuth angle. In this thesis the array is placed along the x axis and with uniform weights ($w_m = 1/N, m = 1, 2..., N$). No consideration has been taken to elevation angles to targets, which means that only azimuthal bearing is calculated. With these assumptions (4.2) reduces to

$$B(\theta,\phi) = \sum_{m=1}^{N} \frac{1}{N} e^{j\frac{2\pi}{\lambda}\cos\phi x_m}\,. \tag{4.3}$$

The beam pattern of an array distributed uniformly along the x axis, with a distance $d = \lambda/2$ between the elements and its center at the origin is shown in Figure 4.1. The *main lobe* or *main beam* is the lobe containing the maximum power, and the width is defined as the angle encompassed between the points where the power has fallen 3 dB below the maximum value. The sidelobes are lobes located outside the main lobe.

By using for example a Chebyshev or a Gaussian window the sidelobes can be suppressed, at the cost of a wider main beam [10], [3]. Figure 4.2 shows an example of a Chebyshev weighting for a constant sidelobe level of -50 dB.

4.2 Spatial covariance matrix

The Spatial Covariance Matrix (SCM) plays an important role in beamforming. It can be used for calculating the power density spectrum in conventional beamforming(section 4.3). It carries information about the correlation between

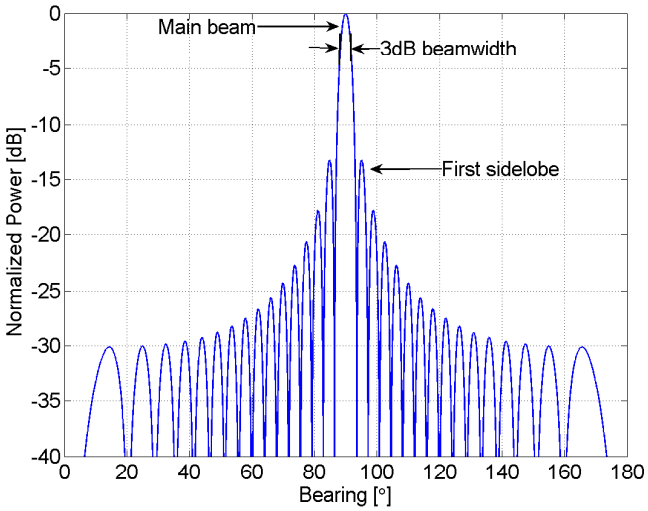

Figure 4.1: Beam pattern for a uniform linear array with 32 elements and $d = \lambda/2$. The main beam, the sidelobes and the beamwidth of the main beam are pointed out.

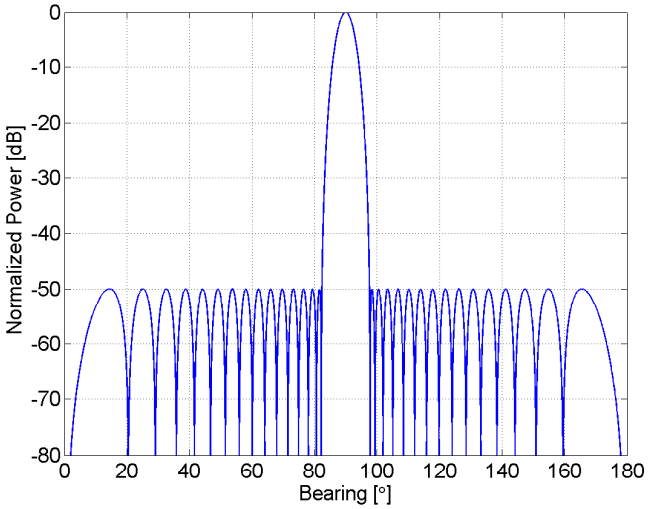

Figure 4.2: Beam pattern for a linear array with 32 elements, $d = \lambda/2$ and a Chebyshev weighting for sidelobes at -50 dB.

the sensors and the phase difference between them. The SCM is defined as

$$\mathbf{R_{xx}} = E\{\mathbf{x}\mathbf{x}^{\mathbf{H}}\} = E\left\{ \begin{array}{ccc} x_1x_1^* & \dots & x_1x_N^* \\ \vdots & \ddots & \vdots \\ x_Nx_1^* & \dots & x_Nx_N^* \end{array} \right\} = \left\{ \begin{array}{ccc} E\{x_1x_1^*\} & \dots & E\{x_1x_N^*\} \\ \vdots & \ddots & \vdots \\ E\{x_Nx_1^*\} & \dots & E\{x_Nx_N^*\} \end{array} \right\} \tag{4.4}$$

where $\mathbf{x} = [x_1, x_2, \dots, x_N]$ is a snapshot vector defined as one sample of data from every sensor at a certain time t_i, and where E is the expectation operator.

The number of snapshot vectors is determined by the amount of incoming data. As the number of snapshots is limited in real applications the SCM must be estimated. That can be carried out in different ways. One way to estimate the SCM is to take the average over the number of snapshots, as

$$\hat{\mathbf{R}}_{\mathbf{xx}} = \frac{1}{M}\sum_{i=1}^{M} \mathbf{x_i}\mathbf{x_i}^H \,, \tag{4.5}$$

where M is the number of snapshots and H is the Hermitian conjugate. The more snapshots that are used for estimating the SCM, the more accurate the estimation will be if the target is stationary in space and time. If the target is moving the number of samples required depends on the movement of the target and the sampling frequency.

When tracking a target for a longer time, many SCMs has to be estimated, and in certain time periods the amount of noise can increase, which means that during that time the SCM will not be accurate. One solution to that problem is to use recursive updating of the SCM as follows

$$\hat{\mathbf{R}}_{\mathbf{xx}} = \alpha\hat{\mathbf{R}}_{\mathbf{xx}}^{(n)} + (1-\alpha)\hat{\mathbf{R}}_{\mathbf{xx}}^{(n-1)} \quad 0 \leq \alpha < 1 \,, \tag{4.6}$$

where α is a constant that determines how much information from the previous SCM should be included in the calculation of the new SCM.

4.3 Conventional beamforming in the far field

Beamforming with plane waves is often used to find the Direction Of Arrival (DOA). Figure 4.3 shows a plane wave $s(t)$ impinging on a linear array of N sensors at time t with the direction ϕ relative to the array. To locate the DOA beamforming is used. Each sensor records the acoustic field from the plane wave. The waveform measured at the mth sensor is denoted by $x_m(t)$ which is given by

$$x_m(t) = s(t + kd\cos\phi) + n_m(t) \,, \tag{4.7}$$

where $k = 2\pi/\lambda$ and $n_m(t)$ is the additive noise due to the medium.

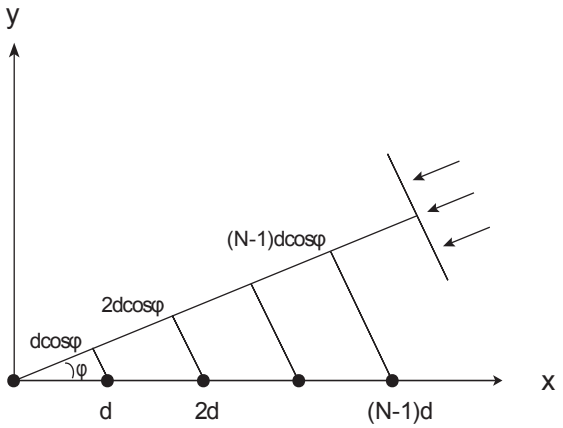

Figure 4.3: Plane wave impinging on a linear array.

The output $y(t)$ of the array can be written as

$$y(t) = \sum_{m=1}^{N} w_m x_m(t - \tau_m)\,, \tag{4.8}$$

where τ_m are delays [14].

By using the information in the time delays at every sensor, a DOA can be estimated. The time delays add either constructively or destructively depending on the phase, and by adding phase shifts to the signals it is possible to simulate the array being steered in different directions. When the signals in each sensor add constructively, a main lobe is formed. The signals will also add constructively in other directions and form lobes, but they will be much weaker and are called sidelobes. The weights can be chosen in different ways depending on the desirable beam pattern (section 4.1). The resolution of the array can be explained by the Rayleigh limit and is discussed in [2].

To find the DOA the beam power in every direction is estimated. The power is a function of the angle, and the angle with maximum power corresponds to the DOA. The beamforming can be performed in either the time domain or the frequency domain, here the frequency domain steps will be discussed. The Fourier transform of (4.8) results in

$$Y(f) = \sum_{m=1}^{N} w_m X_m(f) e^{-j2\pi f \tau_m}\,. \tag{4.9}$$

Equation (4.9) can be written as a product of two vectors as

$$\mathbf{Y}(f) = \mathbf{S^H X}\,, \tag{4.10}$$

where $\mathbf{S}$ is the $N \times 1$ steering vector whose elements are

$$S_m = w_m e^{+j2\pi f \tau_m}\,. \tag{4.11}$$

Every angle ϕ corresponds to a different time delay on each sensor as

$$\tau_m = \frac{kd\cos\phi}{2\pi f}\,. \tag{4.12}$$

Equations (4.11) and (4.12) yields

$$S_m = w_m e^{+jkd\cos\phi}\,. \tag{4.13}$$

The power in the beam as a function of angle is computed by

$$\mathbf{P}(\phi) = E\{|\mathbf{Y}(f)|^2\}\,, \tag{4.14}$$

where E is the expectation operator. Substituting (4.10) into (4.14) yields

$$\mathbf{P}(\phi) = E\{|\mathbf{S^H X}|^2\} = E\{\mathbf{S^H X X^H S}\}\,. \tag{4.15}$$

Assuming that the signal is narrow banded with a frequency f_0 means that the steering vector $\mathbf{S}$ can be considered as constant in (4.15), only dependent on the angle ϕ, and thus can be taken out of the expectation operator. This gives

$$\mathbf{P_{CB}}(\phi) = \mathbf{S^H} E\{\mathbf{X X^H}\}\mathbf{S} = \mathbf{S^H R_{xx} S}\,, \tag{4.16}$$

where $\mathbf{R_{xx}}$ is the covariance matrix (section 4.2)[12]. $\mathbf{P_{CB}}$ is called the conventional beamformer (CB), the Bartlett processor or the sum-delay method

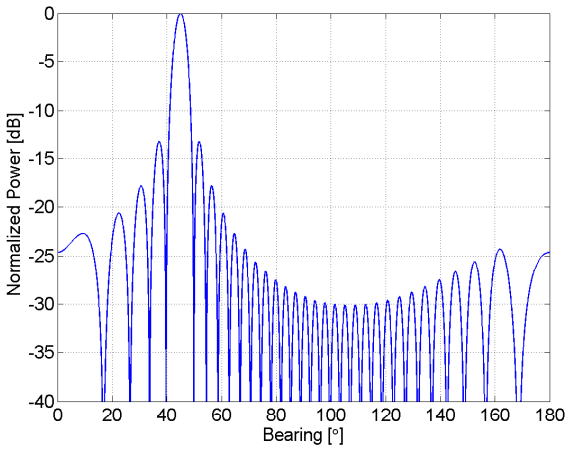

Figure 4.4: The Power-Bearing spectra, estimated with CB. There is a target at 45° relative to end fire of the array. The number of sensors is 32.

[7], [14]. The idea is to vary ϕ and calculate the power according to (4.16). The value of ϕ which yields the maximum power corresponds to the DOA. This is illustrated in Figure 4.4 in which the power is plotted as a function of bearing.

Equation (4.16) is valid for one or several sources at the same frequency. One way to extend the narrow band beamformer into a broad band beamformer is to divide the signals frequency components into blocks and generate narrow band components. The algorithm can then be applied to each block of different frequencies in turn. The conventional beamformer is robust and easy to implement, and the largest sources of errors are the use of inaccurate speeds of sound and inaccurate distances between the sensors.

4.4 MUSIC

MUltiple SIgnal Classification (MUSIC)[13] is a subspace-based method which utilizes a spectral decomposition of the covariance matrix in the analysis. The idea is to separate the received signal into a signal subspace and a noise subspace. The SCM can be decomposed into eigenvectors as

$$\mathbf{R_{xx}}\mathbf{V_i} = \lambda_\mathbf{i}\mathbf{V_i} \qquad i = 1, \ldots, N\,, \tag{4.17}$$

where λ_i is the eigenvalue associated with eigenvector $\mathbf{V_i}$. The eigenvalues are organized in descending order as

$$\lambda_1 \geq \lambda_2 \geq \ldots \geq \lambda_N\,. \tag{4.18}$$

In this thesis the number (d) of large eigenvalues is used as the estimated number of sources. This is done by

$$\hat{d} = \ \text{argmax}\,|\,\text{grad}(\boldsymbol{\lambda})|\,, \tag{4.19}$$

where *grad* is the gradient of the eigenvalues obtained from the SCM. The method for estimating the number of sources is illustrated in Figure 4.5 (a) , which shows the eigenvalues and in Figure 4.5 (b) which shows the absolute value of the gradient.

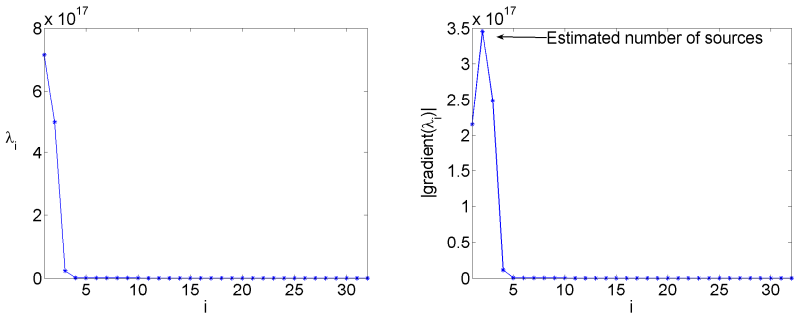

Figure 4.5: Illustration of the eigenvalues and the absolute value of the gradient of the eigenvalues.

The $N - d$ eigenvalues and the corresponding eigenvectors, denoted by $\mathbf{V_{noise}} = [\mathbf{v_{d+1}} \dots \mathbf{v_{N-d}}]$, are assumed to span the noise subspace. The steering vectors for the true sources should be orthogonal to the noise subspace, thus

$$\mathbf{S}(\phi_i)^H \mathbf{V}_{noise} = 0 \quad i = 1 \dots d\,, \tag{4.20}$$

where $\mathbf{S}$ is the steering vector defined in (4.13). The MUSIC cost function P_{MUSIC} is given by

$$P_{MUSIC}(\phi) = \frac{1}{\mathbf{S^H V_{noise} V_{noise}^H S}}\,. \tag{4.21}$$

When the steering vectors are steered to a source P_{MUSIC} will have a sharp peak because the denominator in (4.21) approaches zero. However, the P_{MUSIC} cost function output is *not* a power estimate, as in the conventional beamformer, but rather a measure of the degree of orthogonality between the steering vector and the noise subspace. MUSIC has a better resolution than CB. A comparison between CB and MUSIC is shown in Figure 4.6 using a source at 88° and at 92° relative to end fire of the array. However MUSIC is sensitive to errors in the assumed model, for example with a wrong value of d, the resolution is decreased.

Other criteria can be used for estimating the number of sources, such as Minimum Description Length and Akaike Information Criterion [14], but they are not used in this thesis.

4.5 Beamforming with matched wavefront

If the source is at a distance of

$$R < 2\frac{L^2}{\lambda}\,, \tag{4.22}$$

where R is the distance to the source and L is the length of the array, the array is considered to be in the near field [6]. Without making any adjustments to the beamformer, the performance will be degraded if the wave is assumed to be planar. The time delays between the sensors are now not only determined by the direction, but also by the distance to the source. In this case the wavefront curvature can be detected within the arrays aperture and the sources can be localized both in range and in DOA. Adjusting the steering vectors in the beamformer to the appropriate shape of the wavefront will yield a higher Signal to Noise Ratio (SNR) in the power bearing spectrum than when using

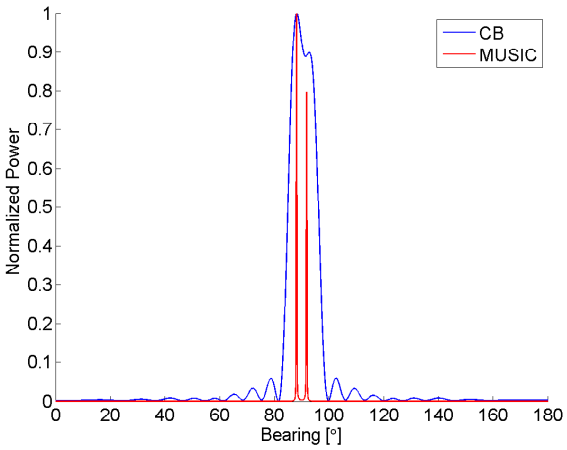

Figure 4.6: The power-bearing spectra, estimated with CB and MUSIC. There is one target at 88° and one at 92° relative to end fire of the array.

a plane wave beamformer because the signals from the sensors will be added more coherently. An example of CB assuming plane waves and a beamformer adjusted for the wavefront is shown in Figure 4.7. The source is at 90° relative to end fire of the array and at a distance of 400 m. Beamforming with the spherical wavefront yields a higher SNR. The SNR in beam space is calculated by dividing the power in the main beam by the power in the rest of the power bearing spectrum below the 3 dB power level as

$$SNR = 10\log(\frac{Power_{mainbeam}}{Power_{below\,3dB power\,level}})\,. \tag{4.23}$$

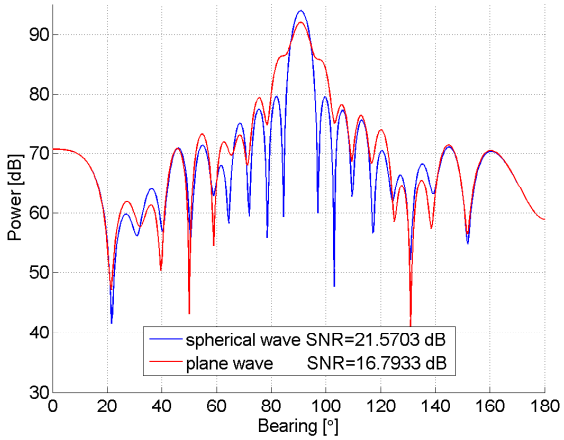

Figure 4.7: Comparison of beamforming with a plane wavefront(red curve) and a spherical wavefront(blue curve) using CB.

4.5.1 Methods for determining the shape of the wavefront

Estimating the shape of the wavefront using time delay estimation

One way to determine the shape of the wavefront is to estimate the Time Difference Of Arrival (TDOA) between sensors. The time delays can be estimated by searching for the maximum value of the cross-correlation function of the observed signals. Let us assume there is a signal received by two sensors

$$\begin{aligned} x_1(t) &= s(t) + v_1(t) \\ x_2(t) &= s(t+D) + v_2(t)\,, \end{aligned} \tag{4.24}$$

where $s(t)$ and $s(t+D)$ are the same signal with a delay D between them and $v_1(t)$ and $v_2(t)$ are additive noise. The cross-correlation function of the signals x_1 and x_2 is defined as

$$X_{corr}(\tau) = \frac{1}{L}\sum_{k=1}^{L} x_1(\frac{k}{f_s})x_2(\frac{k}{f_s}+\tau)\,, \tag{4.25}$$

where $(L-1)/f_s$ is the length of the estimation window and f_s is the sampling frequency. The estimated time lag is then

$$\hat{D} = \ \text{argmax}\, X_{corr}(\tau)\,. \tag{4.26}$$

A plot of a cross-correlation of a narrowband signal is shown in Figure 4.8. The cross-correlation is quasi periodic with the same period as the narrowband signal, and it peaks at the delay $\hat{D}$ corresponding to the time delay between the signals.

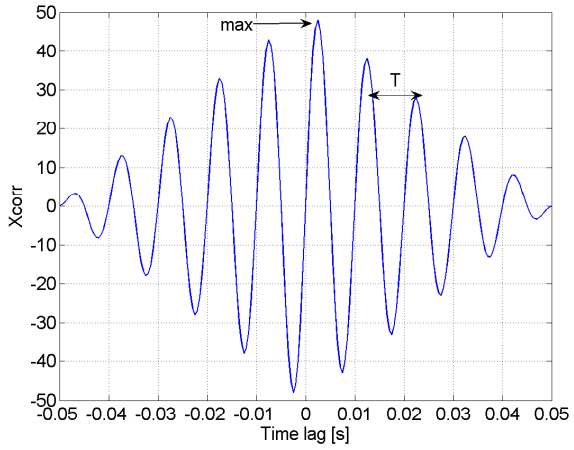

Figure 4.8: Cross-correlation function between two narrow band signals.

The shape of the wavefront is estimated by first estimating the DOA, ϕ_{DOA}, using a plane wave assumption, then steering the array in the direction of the impinging wave by applying appropriate time delays to each sensor. This is sketched in Figure 4.9.

The received signals are assumed to be sinusoidal. This means that it is sufficient to use an estimation window with a length of one period, T when calculating the cross-correlation. Because the desired resolution of the time lags

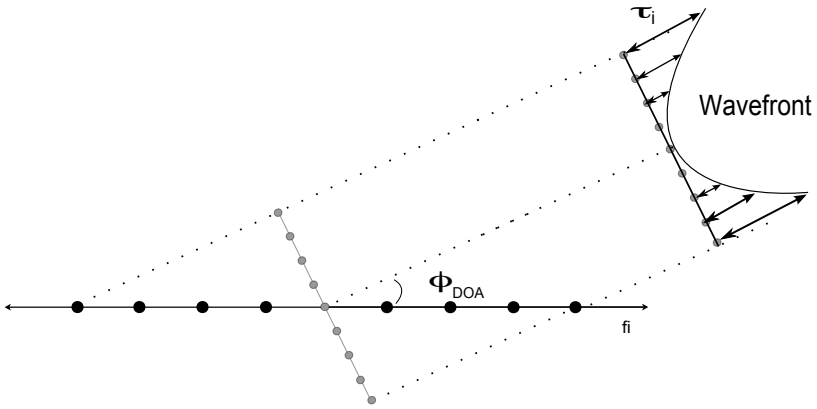

Figure 4.9: Estimating the time delays τ_i by first steering the array in the direction of arrival.

is often much higher than the sampling interval, it is necessary to interpolate the signals $x_i(t)$ before calculating the correlation function. In this thesis a sampling frequency of 3333.33 Hz is used, and when estimating the time delays the signal is interpolated with 20 points between each sample. In order to get an accurate estimation of the time delays, the signal is filtered by a bandpass filter around the frequency of interest. Each time delay estimation is calculated with respect to a reference sensor. In this thesis the reference sensor is sensor 16, which lies in the middle of the array. The estimation of the shape of the wavefront is obtained after all the time delays are estimated with respect to the reference. In order to get a better estimate of the shape, the estimation is made over many wavelengths and then averaged over all estimates. A polynomial fit is used to fit the time differences to a smooth wavefront by constraining its continuity. An example of fitting a wavefront affected by noise is shown in Figure 4.10.

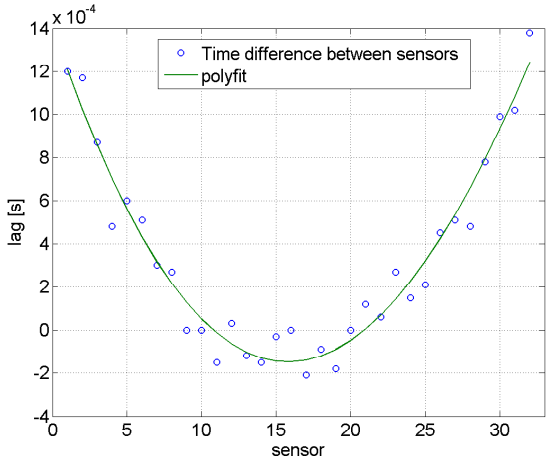

Figure 4.10: Noisy wavefront estimated by a polynomial fit of the time delays.

When the time delays $\boldsymbol{\tau} = [\tau_1, \tau_2, \ldots, \tau_N]$ for the respective sensors are ob-

tained, a new steering vector is created

$$S_{i,matched} = S_i e^{+j2\pi f \tau_i C}\,, \tag{4.27}$$

where $S_{i,matched}$ is the ith element of the steering vector, S_i is the ith element of the plane wave steering vector and C is a correction term defined as

$$C = \frac{\sin\phi}{\sin\phi_{DOA}}\,. \tag{4.28}$$

where ϕ is the steering angle of the array, and ϕ_{DOA} is the incidence angle of the wave. The correction term is used to adjust the estimated time delays for the effective length of the array (see Section 4.6), when the array is steered in different directions. Equations (4.13), (4.27) and (4.28) yield

$$S_{i,matched}(\phi) = w_i e^{+jkd_i\cos\phi + j2\pi f\tau_i\frac{\sin\phi}{\sin\phi_{DOA}}}\,, \tag{4.29}$$

Estimating the distance to the target is carried out by comparing the estimated wavefront curvature to spherical curvatures with different radii. The comparison is made by calculating the differences between the curves as

$$X(R) = \sum_{i=1}^{N}(\tau_{i,est} - \tau_{i,sph}(R))^2\,, \tag{4.30}$$

where $\tau_{i,est}$ is the estimated wavefront and $\tau_{i,sph}(R)$ is the time delays for a spherical wavefront, see (4.32). The estimated distance is

$$\hat{R} = \ \operatorname{argmin} X(R)\,. \tag{4.31}$$

Matching received field to a spherical wavefront

Another way of matching the wavefront is to restrict the wavefront to a spherical shape. The spherical shape of the wavefront is represented by time delays between sensors. As shown in Figure 4.11, the radius of the sphere coincides with the distance to the target. The expression for each time delay is shown in (4.32).

$$\tau_{i,sph}(R) = \frac{-R\overset{+}{_{(-)}}\sqrt{R^2 + (d_i\sin\phi_{DOA})^2}}{c}\,, \tag{4.32}$$

where τ_i is the time lag to sensor i measured from the midpoint of the array, d_i is the distance to the ith sensor, ϕ_{DOA} is the angle of incidence and R is the distance to the source. The formula is derived from Pythagoras theorem. Adjustments to the steering vectors are made by multiplying the elements of the steering vector as

$$S_{i,sph}(R) = S_i e^{+j2\pi f\tau_{i,sph}(R)}\,, \tag{4.33}$$

where $S_{i,sph}$ is the ith component of the steering vector, (4.13), and $\tau_{i,sph}$ is the ith spherical time delay defined in (4.32). Finding the radius is done by calculating the output power of the beamformer over a range of spherical shapes when the array is steered to the DOA. The range yielding maximum power corresponds to the estimated range, as shown in (4.34).

$$\hat{R} = \operatorname{argmax}\mathbf{P}(R,\phi_{DOA})\,, \tag{4.34}$$

where $\mathbf{P}$ is the output power of the beamformer. After the distance estimation is obtained, the steering vector is adjusted to

$$S_{i,sph}(\phi) = w_i e^{+jkd_i\cos\phi + j2\pi\frac{f}{c}(-\hat{R}+\sqrt{\hat{R}^2+(d_i\sin\phi)^2})}\,, \tag{4.35}$$

and with $k = 2\pi f/c$ equation (4.35) becomes

$$S_{i,sph}(\phi) = w_i e^{+jk(d_i \cos\phi - \hat{R} + \sqrt{\hat{R}^2 + (d_i \sin\phi)^2})} . \tag{4.36}$$

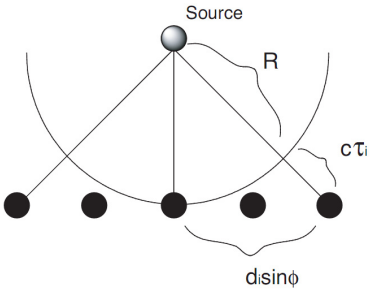

Figure 4.11: A spherical wavefront impinging on an array with 5 elements .

4.6 Effective length of array

The effective length of the array aperture shrinks with the sine of the incidence angle, as shown in Figure 4.12 with a wave approaching at an angle ϕ.

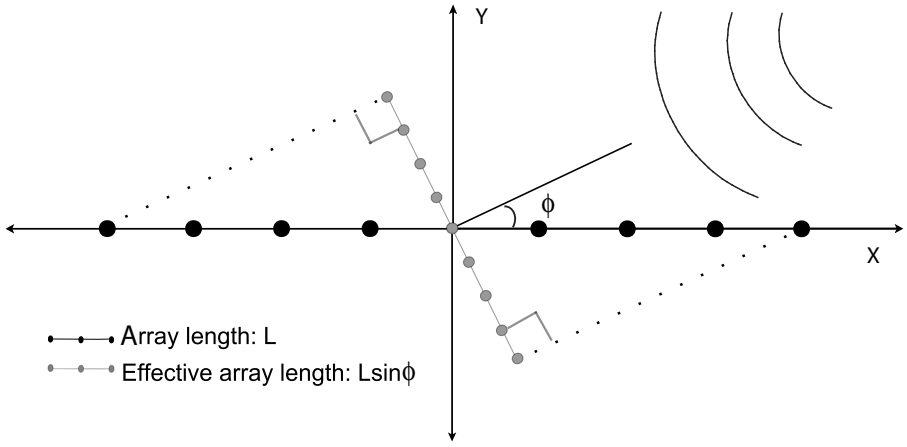

Figure 4.12: The effective lengths dependence of angle.

This means that it is more difficult to detect the curvature of the wavefront if the angle from broadside is large. Equation (4.22) can be rewritten to account for the incidence angle as

$$R < 2\frac{(L\sin\phi)^2}{\lambda} . \tag{4.37}$$

As discussed above, the condition for being in the nearfield of the array shrinks with the incidence angle.

4.7 Limitation

The steering vector in (4.13) possesses an interesting property, namely

$$S_m(\phi) = S_m(-\phi)\,, \tag{4.38}$$

which means that it can not be determined if an incoming wave is coming from the left or from the right of the array, which is illustrated in Figure 4.13.

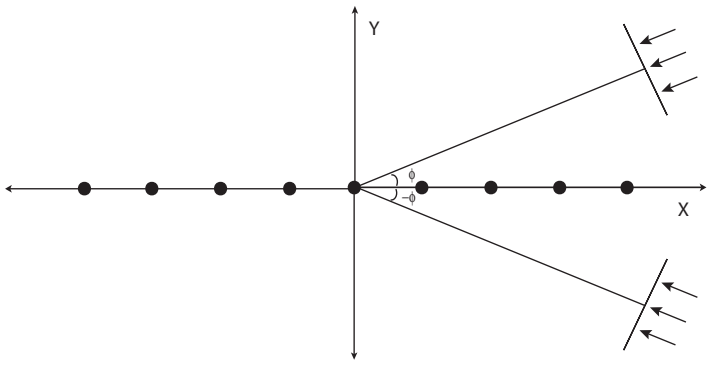

Figure 4.13: Ambiguity of DOA.

This ambiguity is also visible in the beam pattern shown in Figure 4.14, where there is one main lobe at ϕ and one identical, perfectly correlated main lobe at $-\phi$, where ϕ is the incidence angle.

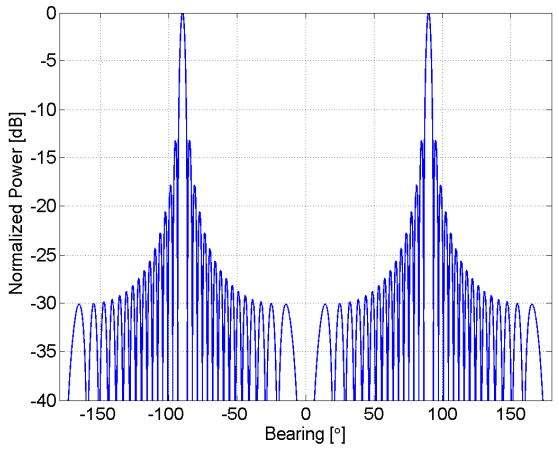

Figure 4.14: Ambiguity in the beam pattern of an array with 32 elements.

5 Data and experimental setup

Both experimental and simulated data were used to evaluate the algorithms discussed in this thesis. The simulated data was generated with Raylab [1], and the experimental data was obtained from a field-test [8].

5.1 Experimental data

The experimental data used in this thesis was obtained from a field experiment conducted in the northern part of Mysingen in the Baltic Sea [8]. A TAS was pulled after a ship, and a stationary sound source emitted tones at different frequencies. The sound source was omni directional with a maximum effect of 170 dB relative to 1 μPa at 1 m.

The array was towed along a rectangular shape and passed the sound source at a distance of 200-750 m (Figure 5.1). The sound source emitted tones at four different frequencies; at 83, 93, 121 and 173 Hz. The hydrophones were suspended at a depth of 15-17 m approximately. The water depth was approximately 40 m. All recorded data were sampled with a sampling frequency of 3.3333 kHz. The TAS contained 32 hydrophones spread over 80 m, and was towed at the end of an 865 m cable.

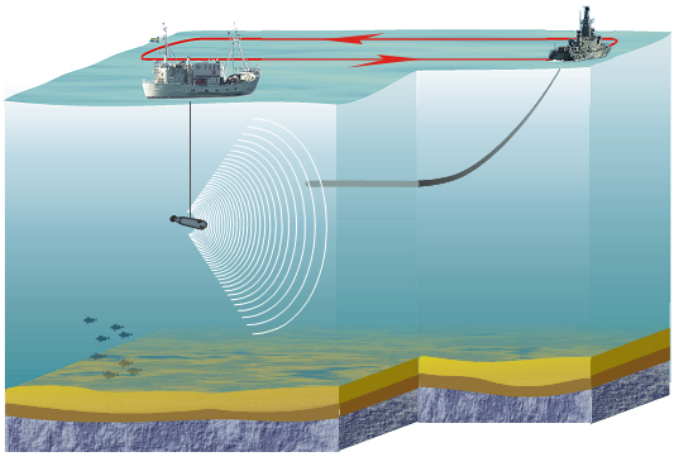

Figure 5.1: Field test setup with a TAS that was carried out in the northern part of Mysingen in the Baltic Sea.

The data from the field-test is divided into 9 runs. Each run consists of travel along a given portion of the track. In this thesis the first two runs are used as test data for the algorithms; the reason being that run 3 is nearly identical to run 1, in run 4 the source power was too low for detection, run 5 had double source tracks, and run 6-9 used a cable 450 m in length, which introduced dominant noise from the ship.

Run 1

The run 1 track consists of a straight segment followed by a sharp turn. During the turn the information about the sensor positions is lost, thus the signal

processing yields no meaningful data. A portion of data collected along the straight portion is used for processing. No GPS data are available for a comparison of the bearing and the distance estimation, therefore a model of the movement is used. The model in (5.1) describes how the angle varies over time,

$$\alpha = \arctan(\frac{vt}{R}) + \alpha_0 \,, \tag{5.1}$$

where v is the speed of the ship, t is the time, R is the distance at Closest Point of Approach (CPA) and α_0 is the angle at CPA. The ship moved with a speed of 8.1 kn and the distance at CPA was approximately 630 m. The source emitted the tones at a power of 160 dB. The angle variation is shown in Figure 5.2 and the movement of the array with respect to the source is illustrated in Figure 5.3.

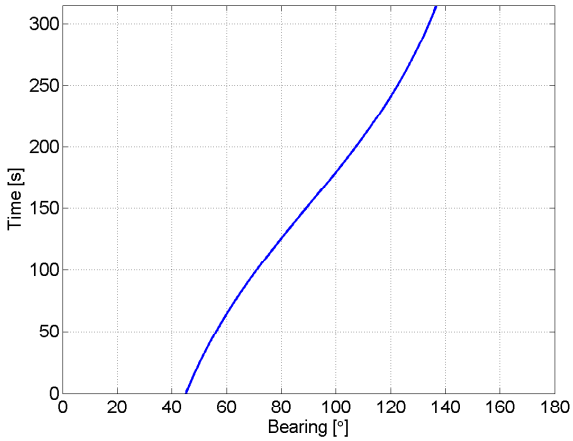

Figure 5.2: Model of how the angle to the target varies over time during run 1.

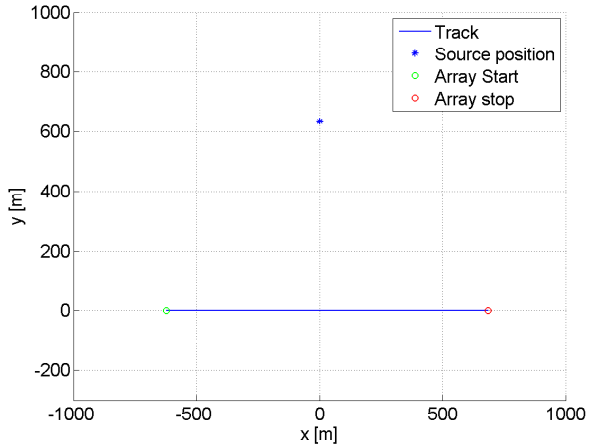

Figure 5.3: Model of the positions of the source and the array during run 1.

The spectrogram of the recorded data, displayed in Figure 5.4, was estimated using a window of 4096 samples and with a 25% overlap. The data is

lowpass filtered with a cut-off frequency of 200 Hz. In the spectrogram all four tones at 83, 93, 121 and 173 Hz are visible. The tone at 173 Hz is used in the analysis of the methods and bearing estimation.

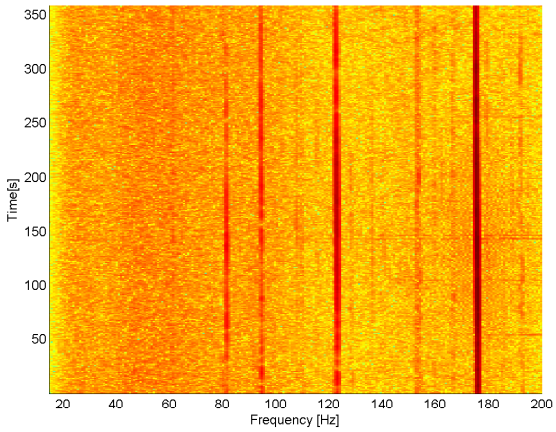

Figure 5.4: Spectrogram for the recorded signal of run 1, estimated using a window of 4096 samples and with a 25% overlap. The signal used for estimating the spectrogram was taken from sensor 1, which was farthest away from the ship pulling the TAS, thus the sensor should contain least amount of noise from the ship.

Run 2

The data segment from run 2 used in the analysis consists of a period when the ship and the TAS travelled along a straight path. The same model describing how the angle varies over time used in the analysis of run 1 is also used here. The ship travelled with the same speed but the distance at CPA was 300 m. The source emitted the tones at a power of 130 dB. The angle variation is shown in Figure 5.5 and the movement of the array with respect to the source is illustrated in Figure 5.3.

The spectrogram of the recorded data is displayed in Figure 5.7. The spectrogram, as in run 1, was estimated using a window of 4096 samples and with a 25% overlap. The data is lowpass filtered with a cut-off frequency of 200 Hz. The data is severely degraded by noise and the four tones at 83, 93, 121 and 173 Hz are hardly visible. The tone at 173 Hz is used in the analysis of the methods and bearing estimation.

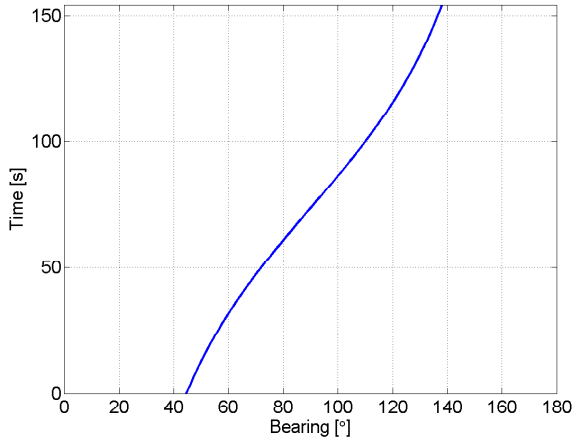

Figure 5.5: Model of how the angle to the target varies over time during run 2.

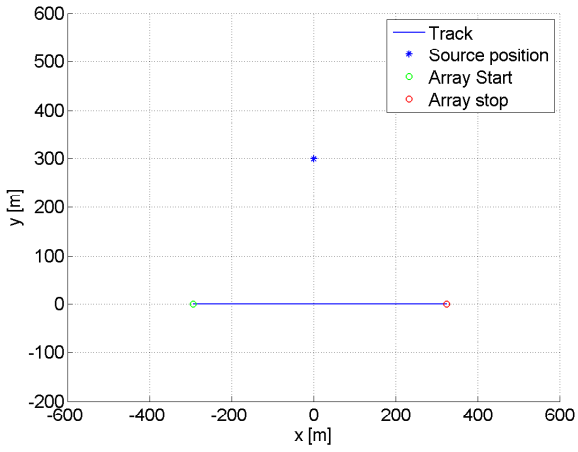

Figure 5.6: Model of the positions of the source and the array during run 2.

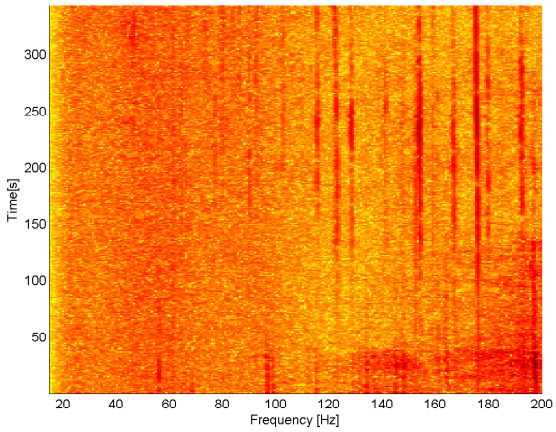

Figure 5.7: Spectrogram for the recorded signal of run 2, estimated using a window of 4096 samples and with a 25% overlap. The signal used for estimating the spectrogram was taken from sensor 1, which was farthest away from the ship pulling the TAS, thus the sensor should contain least amount of noise from the ship.

5.2 Simulated data

Raylab is a simulation program that utilizes ray tracing, see Section 5.2.1. It features a layered environment independent of range and azimuth angle. That implies that the water depth is constant and that the sound speed profile does not vary by range. The bottom is composed of fluid or solid layers, the fluid layers are characterized by three acoustical parameters: sound speed, attenuation and density. The solid layers are characterized by these and two additional parameters: shear speed and shear attenuation. The simulator can simulate moving sources and moving targets. Source signatures can consist of single tones or have a spectral distribution and the directivity of the sources can be selected.

The simulations were constructed so as to reflect the conditions of the field test, which are described in detail in Section 5.1. A shallow water environment and the movement of the array relative to the source were designed to simulate the conditions of run 1 and run 2. The sampling frequency is set to 3333.33 Hz and the source frequency is 173 Hz. The receiving array consists of 32 elements. The speed of the ship towing the TAS is set to 8.1 kn. Uncorrelated normally distributed noise are added to the simulated signals and an SNR value is estimated.

5.2.1 Principles of sound transmission

Sound propagation in a fluid medium can be described mathematically by solutions of the wave equation using appropriate boundary and medium conditions. The wave equation in a Cartesian coordinate system is

$$\frac{\partial^2 p}{\partial t^2} = c(t,x,y,z)^2 \left(\frac{\partial^2 p}{\partial x^2} + \frac{\partial^2 p}{\partial y^2} + \frac{\partial^2 p}{\partial z^2} \right) , \tag{5.2}$$

where x, y and z are the Cartesian coordinates, c is the sound speed in the specific medium, t is the time and p is the acoustic pressure. There are two approaches used frequently to solve the wave equation in a layered medium such as shallow water, Normal-mode theory and Ray theory [15]. In the former the wave propagation is represented by functions called normal modes. Each function satisfies the wave equation for the specific boundary and environment conditions and the functions are summed to form a wave field. Normal-mode approaches are normally used for lower frequencies due to the heavy computational load because the number of modes increases with frequency. In ray theory wave propagation is based on the existence of a wavefront which propagates with the speed of sound in a well-defined direction, and that there is a short distance over which the ray is locally straight. When the ray crosses layers having different speeds of sound the ray is bent toward the layer with lower speed of sound. The angle of refraction depends on the ratio of the speed of sound in the two layers, and is calculated by Snell's law[1]. Ray theory presents a good solution when the variations of the medium, and or the geometry, are small with respect to one wavelength.

When a layer having a lower speed of sound is surrounded by layers with higher speeds of sound, the wave is essentially trapped and a sound channel is formed. The sound wave stays in the channel and can propagate over very long distances with low attenuation. These conditions can arise as a result of warm water at shallow depths, and high salinity and pressure levels at greater

[1] See Appendix B for an illustration of Snell's law

depths, which give rise to higher speeds of sound.

A channel can also be formed in shallow water. The sound propagates by repeated reflections from both surface and bottom. The properties of the surface and the bottom determine how well the wave will propagate.

In this thesis simulations are carried out with Raylab which utilizes Ray theory. The simulated data gives a good indication of the sound propagation even though the frequencies used in the simulations are low, because the variations in the media and geometry are small in the present case. The measured sound speed profile from the field test was used, see Figure 5.8.

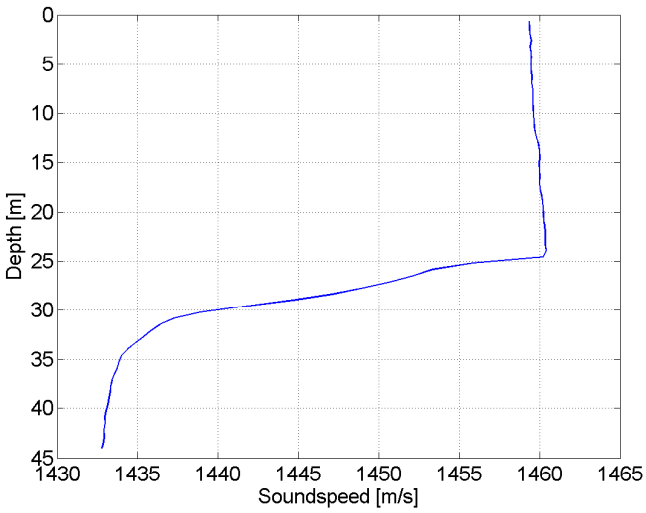

Figure 5.8: Sound speed profile from the field test at Mysingen.

6 Results and analysis

Two methods of adjusting the steering vectors in the beamforming are evaluated: matching to a spherical shape of the wave, and estimating the time difference of arrival between different sensors. These methods are compared to a third method which assumes that the impinging wave is planar.

Data used for the evaluation are described in Chapter 5. The results are displayed as Bearing Time Records (BTR), which displays energy levels in the intervals of $0.1°$ from $0° - 180°$. The BTR is created from several estimated power-bearing spectra. The power-bearing spectra are normalized so that the maximum value of the power spectrum is one. The BTR is then plotted in a colour scale, where red indicates a high value and blue a low value (Figure 6.1).

Figure 6.1: Color scale used in the BTR plots.

The differences between the methods are also assessed numerically by calculating an SNR value, (4.23), from every power-bearing spectrum, then plotting them versus time. The estimated and the real distance are also plotted and the distances are scanned with a interval of 0.5 m from 0 to 3000 m.

6.1 Signal processing

This section describes the signal processing steps performed to estimate the SCMs and the time delays between sensors. Different processing lengths are tested and evaluated to identify a processing window which should be used for the rest of the analysis.

6.1.1 Estimation of SCM

In order for the SCM estimation to be as accurate as possible, the signal should undergo several noise-reducing steps. These steps are illustrated in Figure 6.2. The signal is received at N sensors and an estimation window with 4096 samples is used to estimate the SCM. See Section 6.1.2 for a discussion about the estimation window length. When the signal is truncated to the estimation window it should be windowed to avoid the Gibbs effect. This is done using a Hamming window. The signal is then bandpass filtered around the frequency of interest. A 191st-order FIR filter with a passband chosen to 140-190 Hz is used. The impulse response of the filter is shown in Figure 6.3. Then the signal is converted into a complex-valued signal with the Hilbert transform. The estimation window is divided into 8 blocks of 512 samples each. Each block is Fourier transformed using Fast Fourier Transform (FFT). When the signal blocks are transformed the frequencies corresponding to the signal are found by searching for the peaks in the frequency spectrum. The signal is then filtered in the frequency domain by using only the frequencies corresponding to the signal. A SCM is estimated for each block, and the resulting values are averaged to obtain the final SCM estimate.

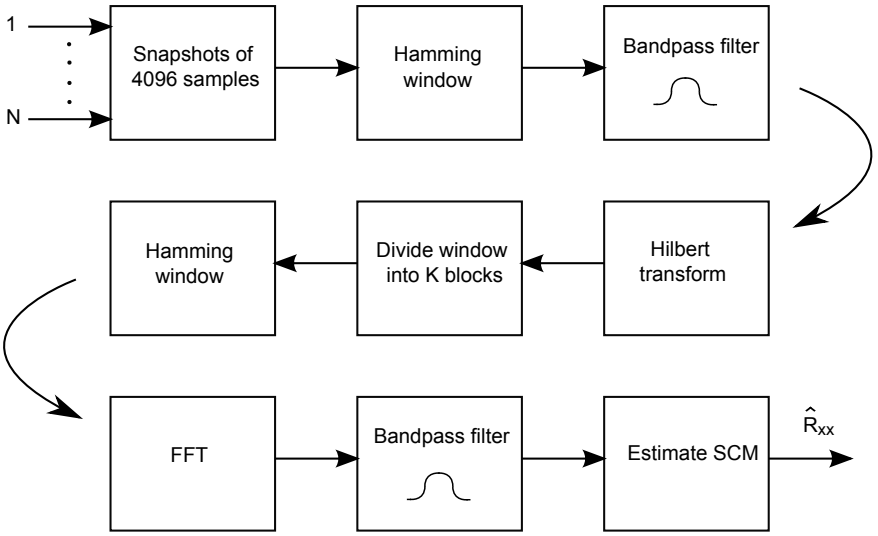

Figure 6.2: Block diagram of the Signal processing steps to estimate the SCM ($\hat{\mathbf{R}}_{\mathbf{xx}}$).

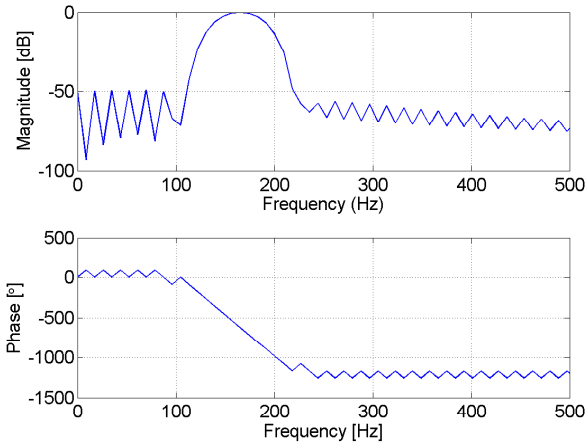

Figure 6.3: Impulse response of bandpass filter.

6.1.2 Length of estimation window and FFT

If the target is stationary with respect to space and time, more data can be used to compute the SCM, thus the estimation will be more accurate. However, the simulation and field-test data used in this thesis is from a non-stationary target, this means that care has to be taken when selecting the size of the estimation window. Choosing the block length and estimation window length as a power of two results in that the FFT calculations can be made effectively. The frequency resolution is given by

$$\Delta f = \frac{f_s}{M}\,, \tag{6.1}$$

where M is the block length and f_s is the sampling frequency. As shown in (6.1) the resolution increases with increasing block length. This is achieved at the expense of a higher variance in the SCM for a fixed window size. There is a trade off between variance in the SCM and the frequency resolution. The sampling frequency used both in the simulated data and the field-test data is 3333.33 Hz. Figure 6.4 illustrates how the resolution varies as a function of block length.

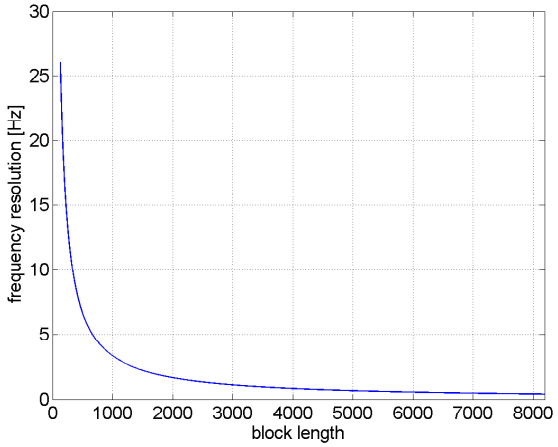

Figure 6.4: Frequency resolution for block lengths from 120 to 8192 samples with a sampling frequency of 3333.33 Hz.

To analyze suitable lengths of the estimation windows and blocks, data from run 1 was used. Three different window sizes were tested: 2048, 4096 and 8192 samples, corresponding to 0.6, 1.2 and 2.4 s. Using a longer estimation window will result in time-lagging between estimated source position due to the big time differences between estimation windows assuming no overlap between the windows, when the source is moving. Using a shorter window results in poorly conditioned covariance matrices. For every window size various block lengths (256, 512, 1024, 2048 samples) were tested. The combinations were evaluated based on the condition number of the covariance matrix and how well the power bearing spectrum is formed. In Section 4.5 the definition of SNR in a power bearing spectra can be found. The condition numbers of the covariance matrices and the SNR for different block lengths for estimation window sizes of 2048, 4096 and 8192 samples are listed in Figure 6.5. The frequency resolution using a block length of 256 samples is poor and yields a low SNR in the power bearing spectra. Block lengths over 256 samples give approximately the same SNR for the different window sizes, but the condition numbers vary. A window size of 4096 samples with a block length of 512 yields a good SNR and a low condition number. Similar results are achieved for a window size of 8192, but a window size of 4096 samples gives a better time resolution, which translates to better tracking. Thus, for the remainder of the analysis an estimation window of size 4096 and block length of 512 samples are used.

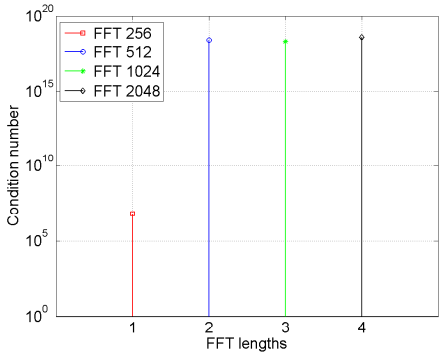

(a) Condition number for a window size of 2048.

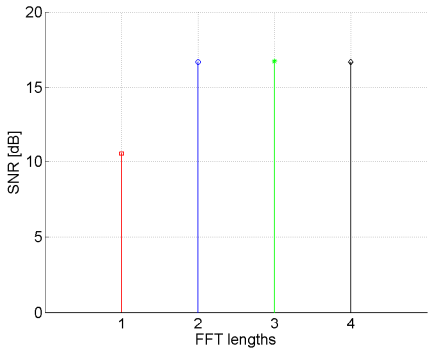

(b) SNR for a window size of 2048.

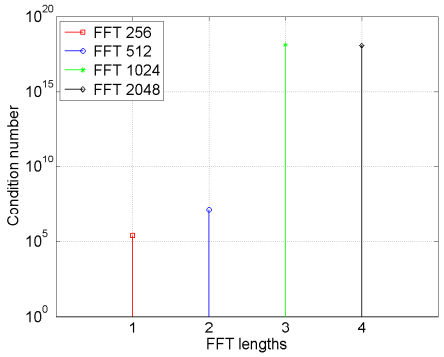

(c) Condition number for a window size of 4096.

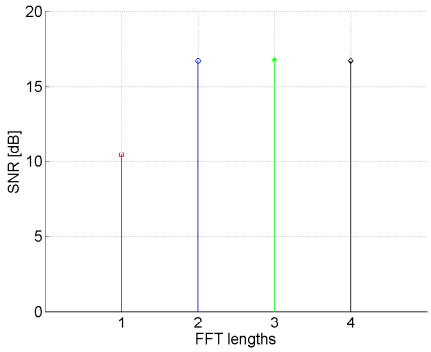

(d) SNR for a window size of 4096.

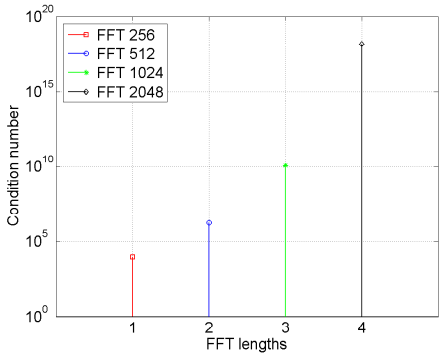

(e) Condition number for a window size of 8192.

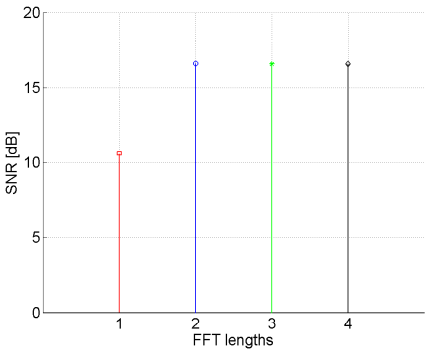

(f) SNR for a window size of 8192.

Figure 6.5: Condition number and SNR for three different window sizes, 2048, 4096 and 8192 samples.

6.1.3 Estimation of time delays

The steps for estimating the time delays between sensors are shown in Figure 6.6. First, the received estimation window is windowed and bandpass filtered using the same filter and window function as in Section 6.1.1. Because the required resolution of the time delays between sensors is much finer than the sampling interval, it is necessary to interpolate the signal. This is carried out by a spline interpolation with 20 points between every sample. The array

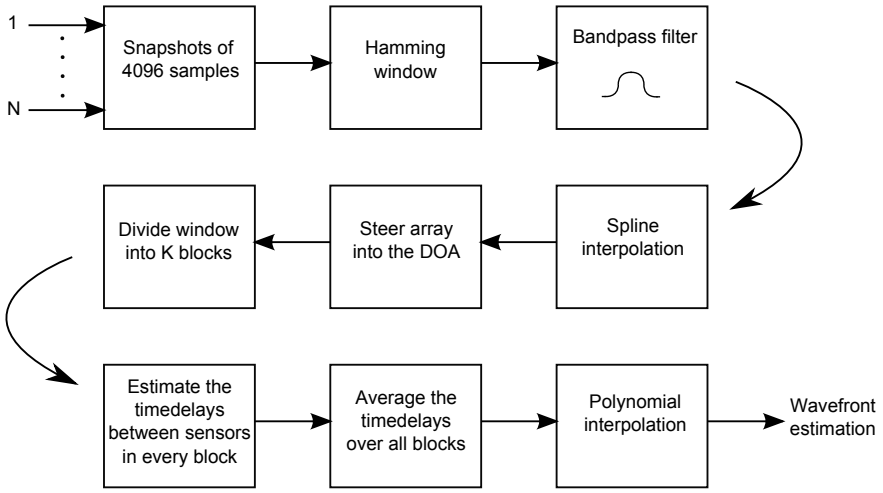

Figure 6.6: Block diagram of the signal processing steps when the time delays are estimated.

is then steered in the direction of the impinging wave by applying appropriate time delays to respective sensors, according to the angle of arrival, see (4.12). Finally, the correlation functions between sensors over a length corresponding to one wavelength are calculated to give estimates of the time delays. Improved estimates are obtained by dividing the estimation window into P blocks and repeating the correlations in every block and then averaging the estimates. In this thesis 20 blocks are calculated and averaged. A polynomial fit of order 3 is then used to approximate the wavefront.

6.2 Distance estimation using the wavefronts curvature

The curvature of the wavefront becomes increasingly difficult to detect the closer the impinging angle is to the endfire of the array and the farther away the target is. As the distance increases, the time delays between sensors shrink quickly, and noise affecting the signals has a greater impact on the estimation. The range resolution of an array is discussed in [2]. Figure 6.7 illustrates the time difference between adjacent sensors depending on the distance to the target and the DOA. A distance estimation from a simulation using Raylab is shown in Figure 6.8 using spherical matching. The target moves away from the array with a constant speed of 8 knots starting from 250 m back to 1500 m for the angles 45° and 90°. Normally distributed uncorrelated noise have been added to the signals from Raylab and the SNR is estimated to 15 dB. The distance estimation worsens as the distance increases. The estimation is more accurate when the target is at 90° than when it is at 45°.

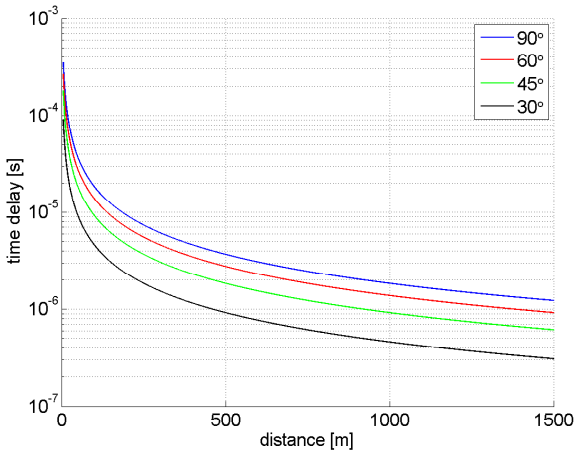

Figure 6.7: Time delays between adjacent sensors for various angles of arrival.

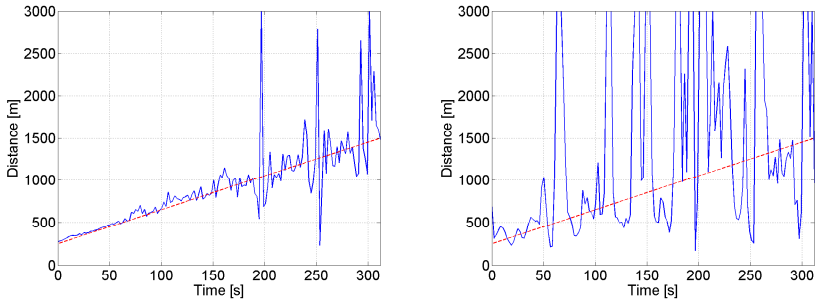

Figure 6.8: Distance estimation with at target moving away at 90° (left) and at 45° (right). The red curve is the real distance.

6.3 Analysis of simulated data

The simulated data from Raylab was configured to emulate the movement of the array relative to the signal source in the field-test (see Section 5.1 and Figure 5.3). Plots of the BTRs, the estimated distances, and the SNRs in the beam space for all the methods are shown in Figures 6.9-6.16. Each Figure shows a comparison between a matched beamforming method, either spherical or time delay, and plane wave beamforming. This section shows results for the array passing the source at $45° - 135°$ for 300 and 600 m at CPA. No recursive updating of the SCM has been used in this section. CB was used in the analysis.

$45° - 135°$ and 600 m at CPA

This section addresses results when the distance at CPA is 600 m. The results of spherical matching versus plane wave beamforming are shown in Figure 6.9. The spherical wavefront method generates a higher received power than plane wave beamforming because the signals are added more in phase. This is evidenced by the fact that there are no sidelobes visible in the BTR for the matched wavefront, whereas for the plane wavefront there is a light blue track near the bearing track. The BTRs are normalized so that the maximum value in every power-bearing spectrum is 1, which means that the sidelobe levels are essentially suppressed depending on the power in the look direction. The distance estimation is accurate when the target is near broadside of the antenna, in bearings between 70° and 110° which occurs approximately between 100 and 200 s. This is also the range in which the SNR in beam space is increased compared to the plane wave assumption. This is because the effective length[1] increases near broadside which yields a better estimation of the wavefront.

The results of the time delay matched beamforming versus the plane wave beamforming are shown in Figure 6.10. The matched wavefront is estimated by using the time delays between the sensors[2]. The BTR and increase in SNR in beam space are similar between the spherical matching and the time delay methods. The distance estimation is biased, and the error near broadside is approximately 300 m.

[1] For a definition of effective length see Section 4.6
[2] See Section 4.5.1

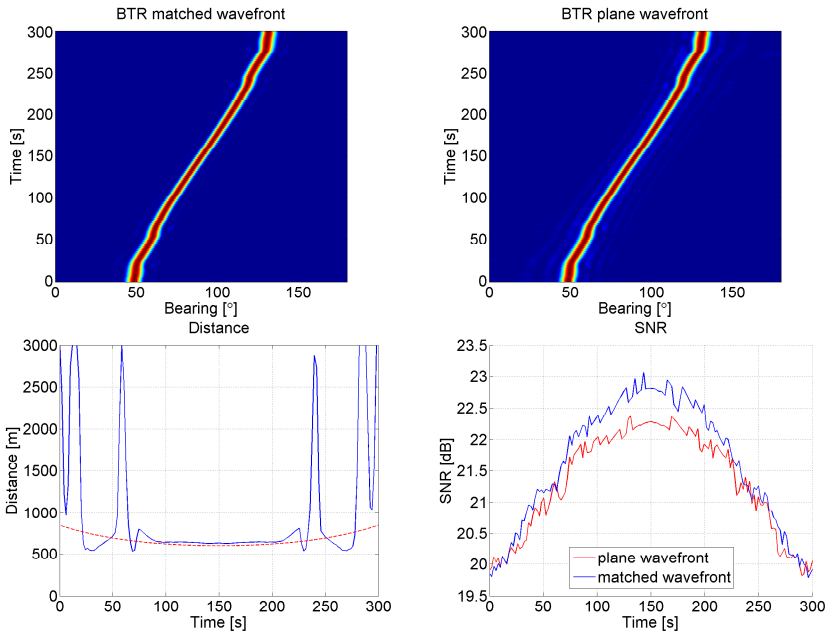

Figure 6.9: BTR estimated with CB using a match to a spherical (top left) and a plane (top right) wavefront. Estimated distance (blue) and real distance (red), bottom left. SNR in beam space for the matched and the plane wavefront, bottom right. No added noise, the distance at CPA is 600 m, and no recursive updating of SCM.

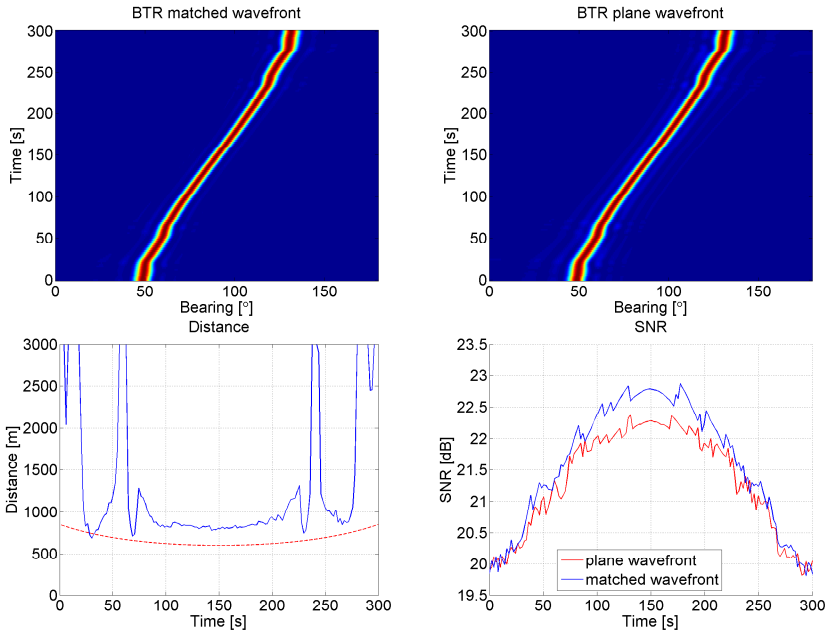

Figure 6.10: BTR estimated with CB using a match by time delay estimates (top left) and to a plane (top right) wavefront. Estimated distance (blue) and real distance (red), bottom left. SNR in beam space for the matched and the plane wavefront, bottom right. No added noise, distance at CPA is 600 m, and no recursive updating of SCM.

$45^\circ - 135^\circ$ and 300 m at CPA

This section addresses results when the distance at CPA is 300 m. The benefits of using a matched wavefront method instead of a plane wave beamforming increase when the source is closer, because the curvature of the wavefront is greater.

In Figures 6.11-6.12, comparison between spherical matching and time delay matching to plane wave beamforming, are shown. There are significant differences in the BTRs between matched beamforming and plane wave beamforming. The matched beamforming methods show a much clearer trace with lower sidelobes than the plane wavefront because the signals are added more coherently. The distance estimation is highly accurate, with an error of approximately 20-40 m near broadside. When the target is near endfire the error increases. The SNR in beam space is up to 2.5 dB higher when using the matched beamformer rather than the plane wave beamformer.

The results of adding normally-distributed uncorrelated noise to the signals are shown in Figures 6.13 and 6.14, and the SNR is estimated to 10 dB. The distance estimation is still accurate for the spherical matching and the high value of the SNRs in beam space indicate the benefits of using a matched beamformer when the target is in the near field of the array.

Consequences of increasing the noise level to an SNR of 5 dB were also studied. The results are shown in Figures 6.15 and 6.16. At this SNR level there are almost no differences between the matched beamformers and the plane wave beamformer. The distance estimations are inaccurate and the differences between the SNRs in beam space of the matched and plane wave beamformers are small.

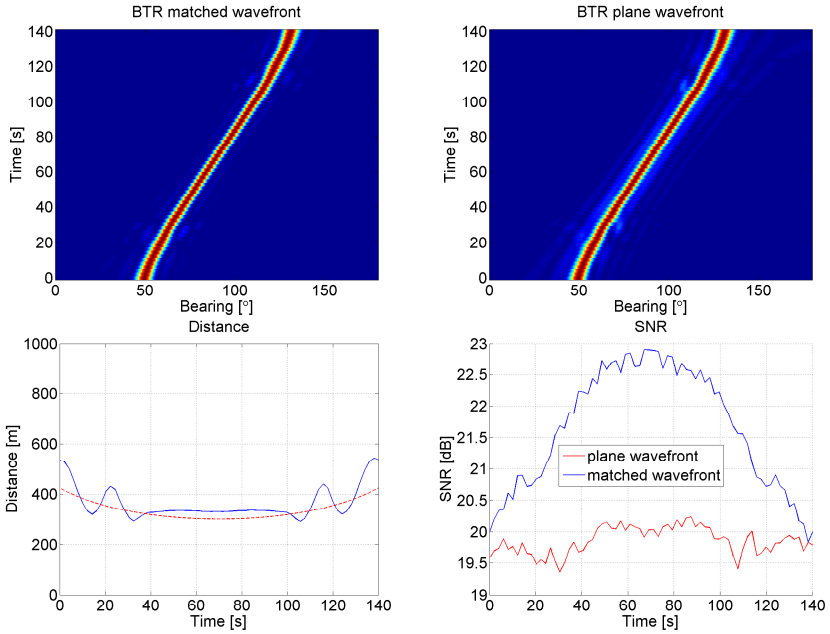

Figure 6.11: BTR estimated with CB using a match to a spherical (top left) and a plane (top right) wavefront. Estimated distance (blue) and real distance (red), bottom left. SNR in beam space for the matched and the plane wavefront, bottom right. No added noise, distance at CPA is 300 m, and no recursive updating of SCM.

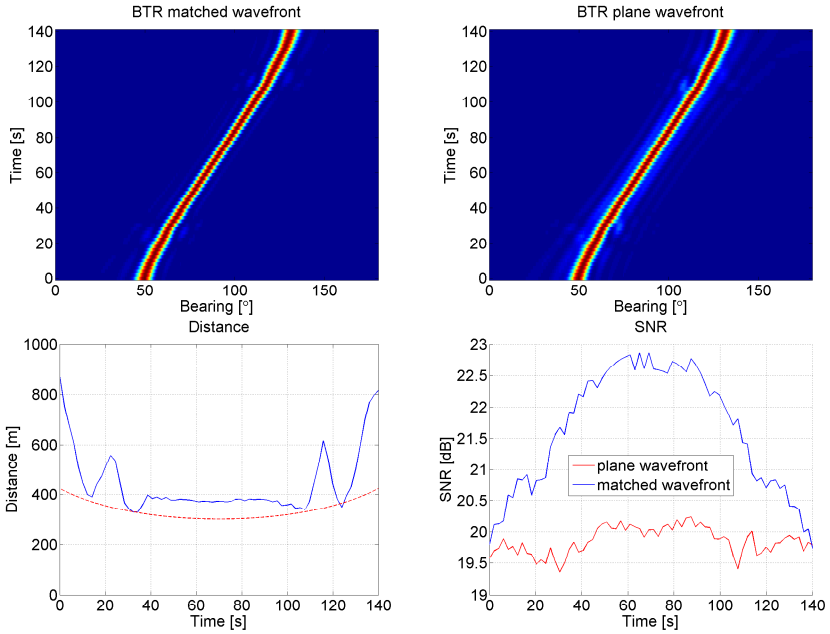

Figure 6.12: BTR estimated with CB using a match by time delay estimates (top left) and to a plane (top right) wavefront. Estimated distance (blue) and real distance (red), bottom left. SNR in beam space for the matched and the plane wavefront, bottom right. No added noise, distance at CPA is 300 m, and no recursive updating of SCM.

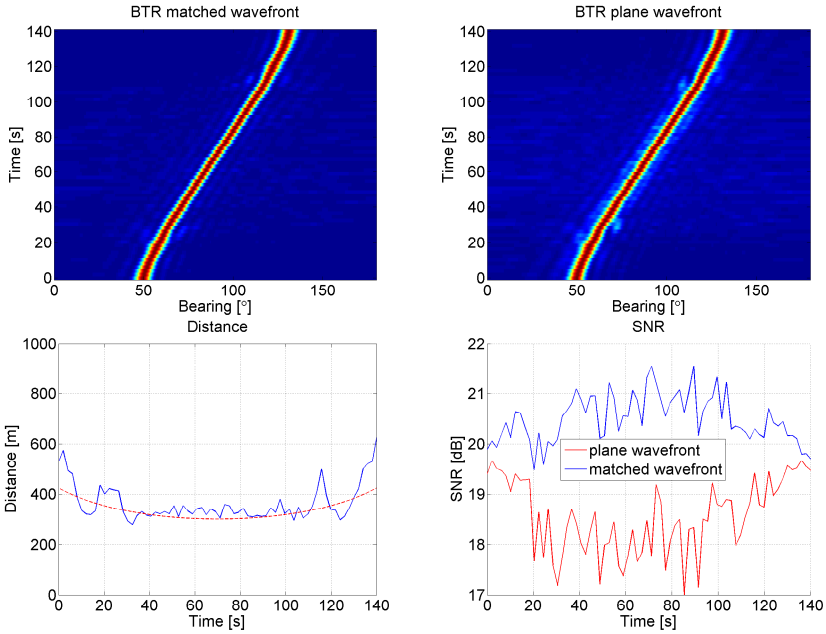

Figure 6.13: BTR estimated with CB using a match to a spherical (top left) and a plane (top right) wavefront. Estimated distance (blue) and real distance (red), bottom left. SNR in beam space for the matched and the plane wavefront, bottom right. SNR is 10 dB, distance at CPA is 300 m, and no recursive updating of SCM.

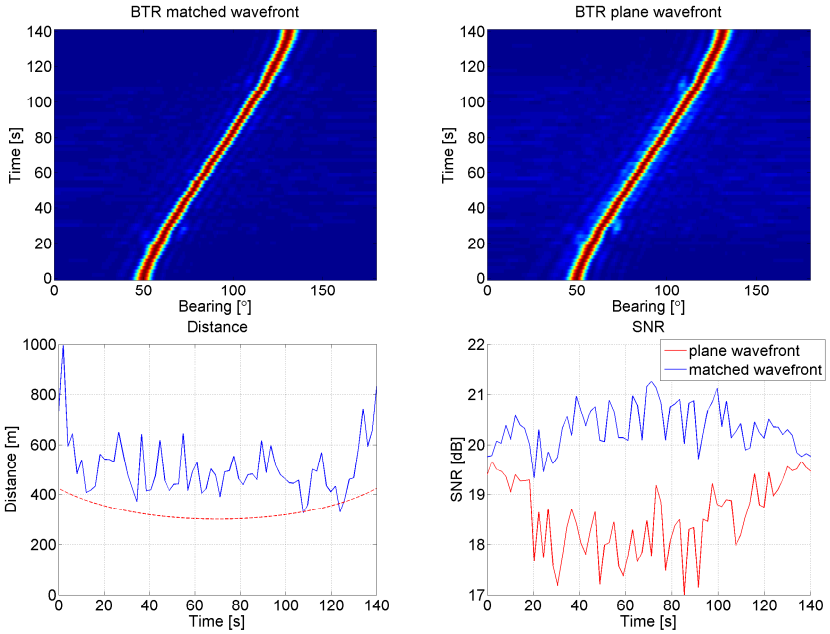

Figure 6.14: BTR estimated with CB using a match by time delay estimates (top left) and to a plane (top right) wavefront. Estimated distance (blue) and real distance (red), bottom left. SNR in beam space for the matched and the plane wavefront, bottom right. SNR is 10 dB, distance at CPA is 300 m, and no recursive updating of SCM.

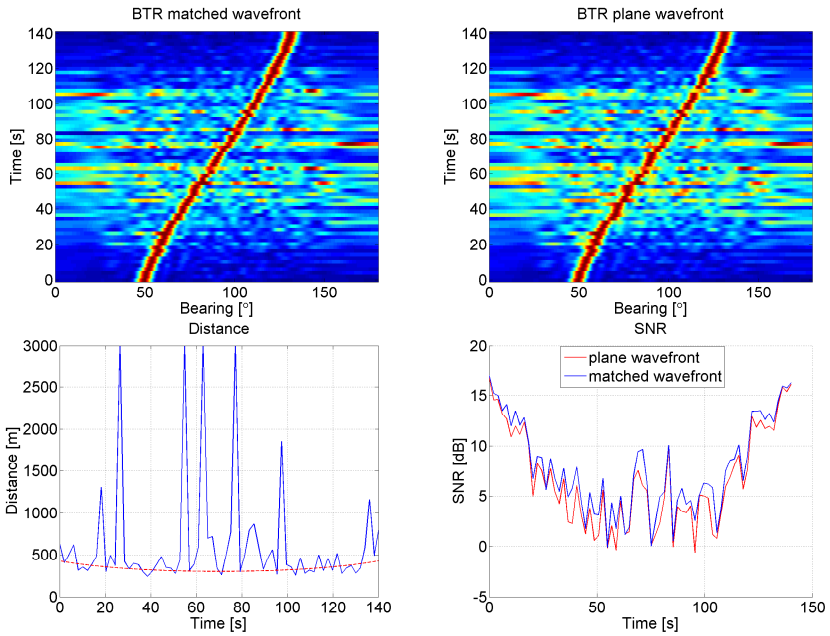

Figure 6.15: BTR estimated with CB using a match to a spherical (top left) and a plane (top right) wavefront. Estimated distance (blue) and real distance (red), bottom left. SNR in beam space for the matched and the plane wavefront, bottom right. SNR is 5 dB, distance at CPA is 300 m, and no recursive updating of SCM.

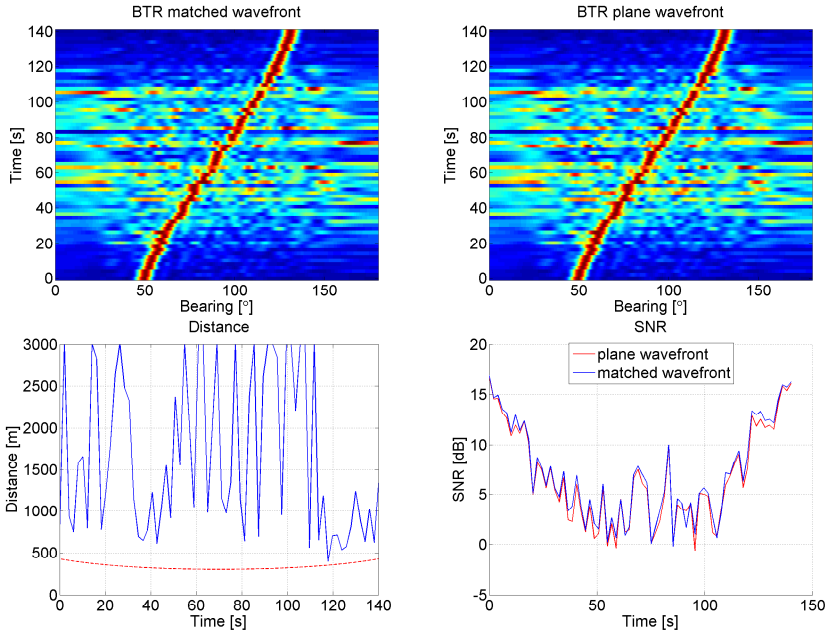

Figure 6.16: BTR estimated with CB using a match by time delay estimates (top left) and to a plane (top right) wavefront. Estimated distance (blue) and real distance (red), bottom left. SNR in beam space for the matched and the plane wavefront, bottom right. SNR is 5 dB, distance at CPA is 300 m, and no recursive updating of SCM.

6.4 Analysis of field-test data

6.4.1 Run 1

During the following analysis the sinusoid with the highest frequency is used, because it generates the largest near field, see (4.22) and (4.37). The near field of the array for a signal with a frequency of 173 Hz is plotted in Figure 6.17. The source is outside the near field of the array at the beginning and end of the data segment, and at these positions the wavefronts are approximately planar. CB and MUSIC were tested in the analysis.

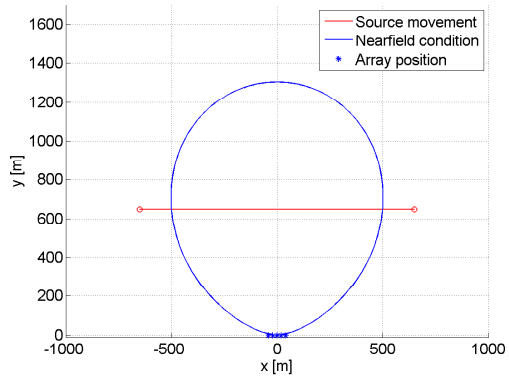

Figure 6.17: Near field of the array used in the field-test with a frequency of 173 Hz.

6.4.1.1 Beamforming using CB

Plots of the BTRs, the estimated distances, and the SNRs in beam space for all the methods are shown in Figures 6.18-6.21. Each figure shows a comparison between a matched beamforming method, either spherical or time delay, and plane wave beamforming. The results of the spherical matching and the plane wavefront beamforming are compared in Figure 6.18. No simulated noise is added and the SNR is estimated to 25 dB. The sidelobes are lowered when using a spherical wavefront which is seen in the BTR plots. The estimated distance has an maximum error of approximately 300 m near broadside. The SNR in beam space is increased by 0.5-1 dB near broadside compared to a plane wave beamformer.

The corresponding plots are shown for time delay matching in Figure 6.19. The distance estimation is less accurate than the corresponding spherical matching. No simulated noise is added and the SNR is estimated to 25 dB.

Figures 6.20 and 6.21 show results when normally distributed uncorrelated noise is added to degrade the data so that the SNR level is 10 dB. The difference in SNR in beam space between plane and matched beamforming has decreased, and the distance estimation has been degraded, especially for the time delay method.

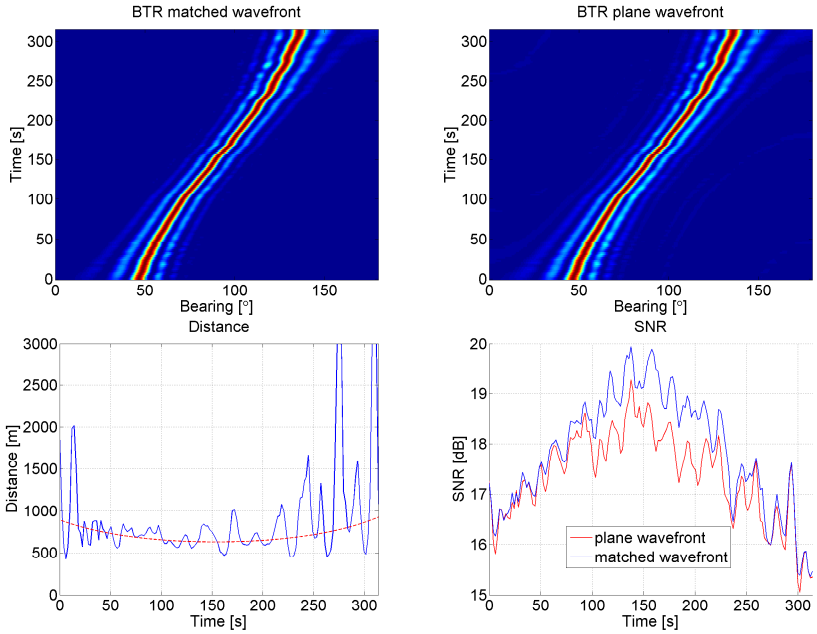

Figure 6.18: BTR estimated with CB using a match to a spherical (top left) and a plane (top right) wavefront. Estimated distance (blue) and real distance (red), bottom left. SNR in beam space for the matched and the plane wavefront, bottom right. No added noise, distance at CPA is 630 m, and no recursive updating of SCM.

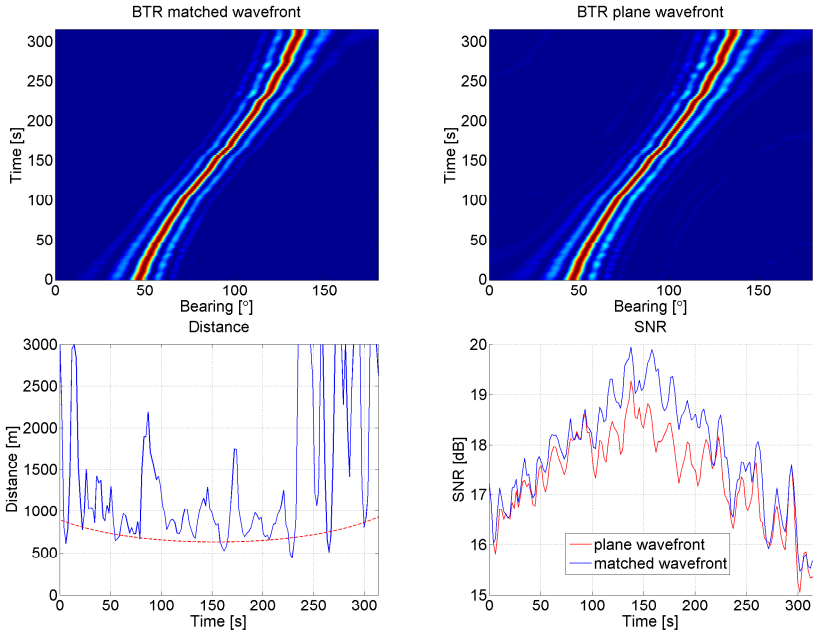

Figure 6.19: BTR estimated with CB using a match by time delay estimates (top left) and to a plane (top right) wavefront. Estimated distance (blue) and real distance (red), bottom left. SNR in beam space for the matched and the plane wavefront, bottom right. No added noise, distance at CPA is 630 m, and no recursive updating of SCM.

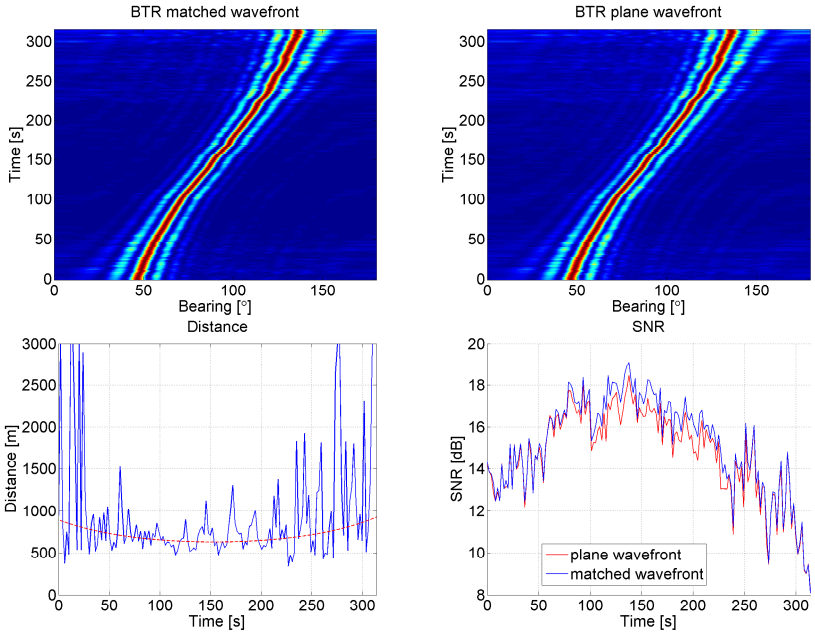

Figure 6.20: BTR estimated with CB using a match to a spherical (top left) and a plane (top right) wavefront. Estimated distance (blue) and real distance (red), bottom left. SNR in beam space for the matched and the plane wavefront, bottom right. SNR is 10 dB, distance at CPA is 630 m, and no recursive updating of SCM.

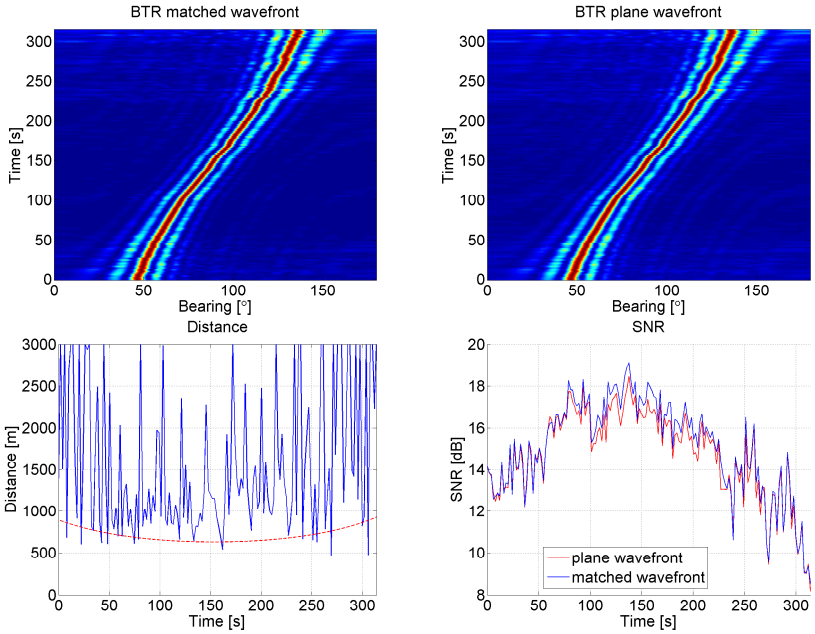

Figure 6.21: BTR estimated with CB using a match by time delay estimates (top left) and to a plane (top right) wavefront. Estimated distance (blue) and real distance (red), bottom left. SNR in beam space for the matched and the plane wavefront, bottom right. SNR is 10 dB, distance at CPA is 630 m, and no recursive updating of SCM.

6.4.1.2 Beamforming using MUSIC

MUSIC gives a sharper main lobe than CB. The output of the beamformer is not a true power spectrum. MUSIC also requires information regarding the number of sources[3]. The number of sources estimations for run 1 with and without added noise are shown in Figure 6.22. The estimation of sources is correct all throughout run 1. Figures 6.23-6.26 display the results of using the MUSIC cost function in the beamforming algorithm. Each figure shows a comparison between a matched beamforming method, either spherical or time delay, and plane wave beamforming.

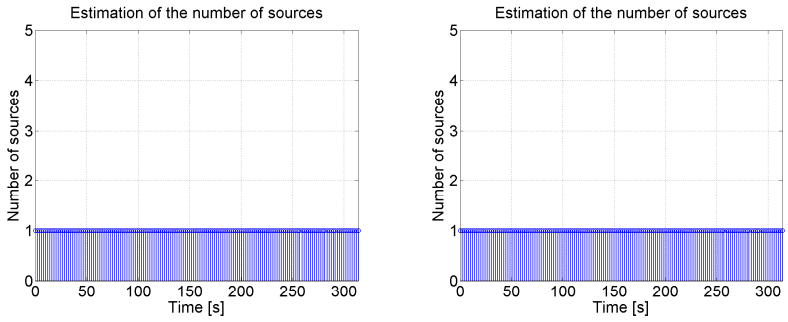

Figure 6.22: Estimation of the number of sources for run 1. No added noise (left), added noise and SNR estimated to 10 dB (right).

The results of spherical matching and plane wavefront beamforming are compared in Figure 6.23. The bearing track is significantly sharper using MUSIC than when using CB. There are more darker regions(dark blue means a low value, see Figure 6.1) in the BTR for the spherical match than in the BTR for the plane wavefront. The distance estimation using CB and MUSIC are exactly the same. Note that the SNR values in beam space for MUSIC are generally lower than those of CB, and that there is no connection to the received power, because the output from the MUSIC cost function is not a power estimate. The important thing to notice is the difference in SNR values between a plane wave front and the matched wavefront. At broadside there is approximately 2 dB difference between spherical matching and the plane wave beamformer.

Corresponding plots for time delay matching are shown in Figure 6.24. The distance estimation is less accurate than for the spherical matching.

Figures 6.25 and 6.26 shows the results for when normally uncorrelated noise has been added to degrade the signals. The BTRs from the matched beamformers show similar results as the plane wave beamformers and the SNRs in the beam space are similar to the plane wave beamformer.

[3]See Section 4.4

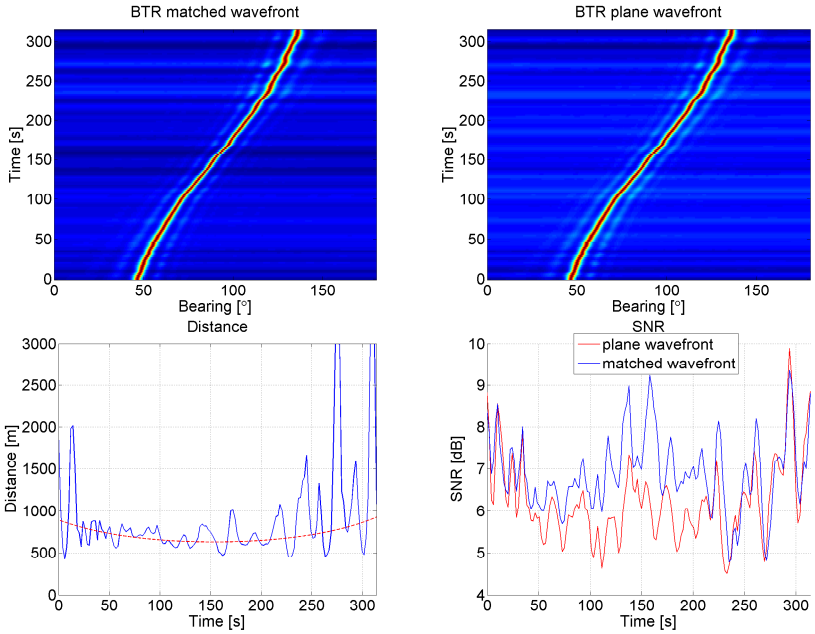

Figure 6.23: BTR estimated with MUSIC using a match to a spherical (top left) and a plane (top right) wavefront. Estimated distance (blue) and real distance (red), bottom left. SNR in beam space for the matched and the plane wavefront, bottom right. No added noise, distance at CPA is 630 m, and no recursive updating of SCM.

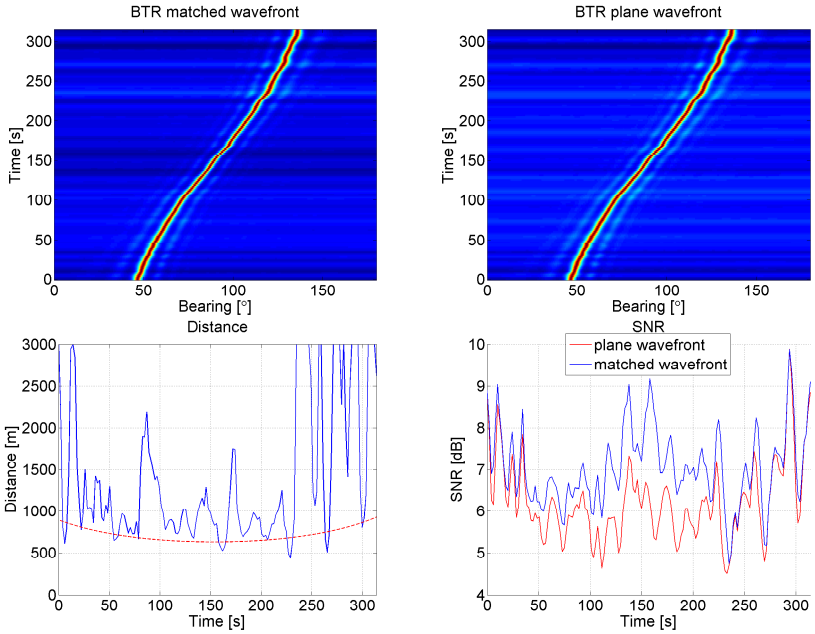

Figure 6.24: BTR estimated with MUSIC using a match by time delay estimates (top left) and to a plane (top right) wavefront. Estimated distance (blue) and real distance (red), bottom left. SNR in beam space for the matched and the plane wavefront, bottom right. No added noise, distance at CPA is 630 m, and no recursive updating of SCM.

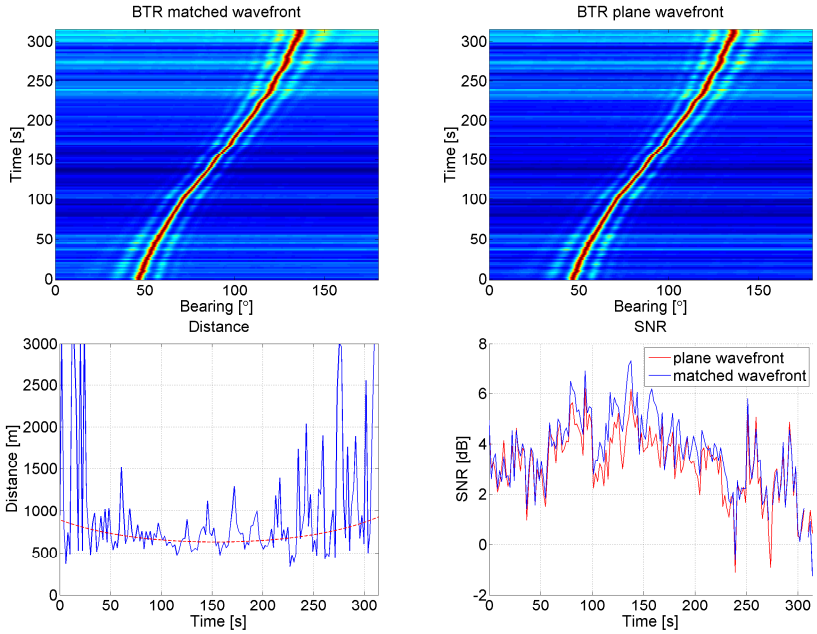

Figure 6.25: BTR estimated with MUSIC using a match to a spherical (top left) and a plane (top right) wavefront. Estimated distance (blue) and real distance (red), bottom left. SNR in beam space for the matched and the plane wavefront, bottom right. SNR is 10 dB, distance at CPA is 630 m, and no recursive updating of SCM.

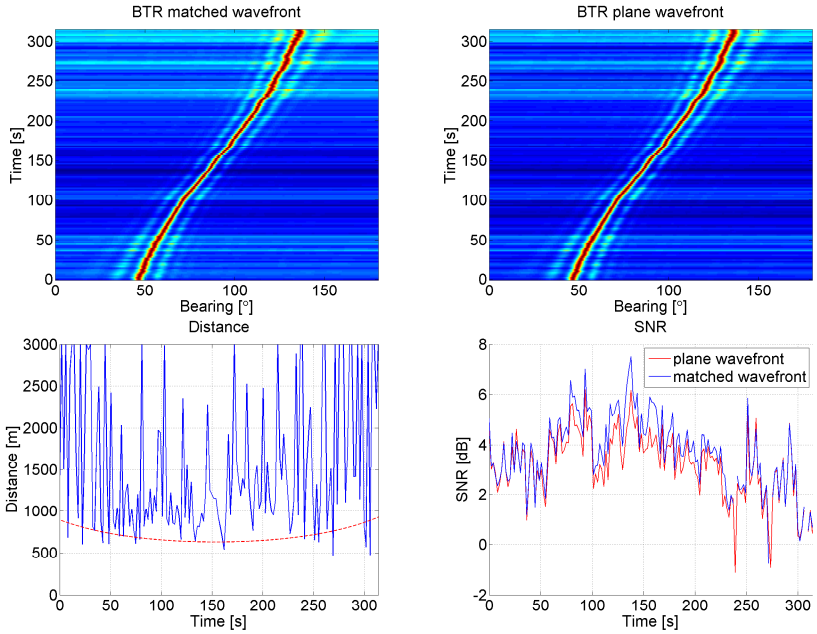

Figure 6.26: BTR estimated with MUSIC using a match by time delay estimates (top left) and to a plane (top right) wavefront. Estimated distance (blue) and real distance (red), bottom left. SNR in beam space for the matched and the plane wavefront, bottom right. SNR is 10 dB, distance at CPA is 630 m, and no recursive updating of SCM.

6.4.2 Run 2

The distance at CPA was approximately 300 m. There was a significant amount of noise present. The estimated SNR for run 2 is shown in Figure 6.27. The SNR was estimated by calculating the energy in the peak at the 173 Hz tone in the frequency spectrum, then dividing that value with the noise level surrounding the peak. MUSIC and CB were tested in the analysis. The signals were processed both with recursive updating, using a constant[4] α of 0.5 due to the high noise levels, and without recursive updating.

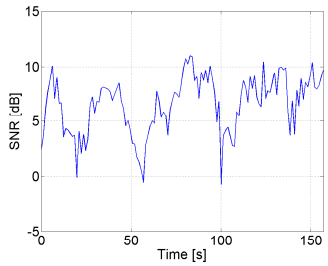

Figure 6.27: Estimated SNR for run 2.

6.4.2.1 Beamforming using CB

Plots of the BTRs, the estimated distances, and the SNRs in beam space for all the methods are shown in Figures 6.28-6.31. Each figure shows a comparison between a matched beamforming method, either spherical or time delay, and plane wave beamforming.

The results of the spherical matching and the plane wavefront beamforming are compared in Figure 6.28, both obtained without recursive updating. There are differences in the BTRs, for example at 100 s where the matched beamforming manages to follow the target better than the plane wave beamformer. The estimated distance error is large and the SNR in beam space oscillates significantly. The same drops are observed at 50 and 100 s in the SNR estimation and the SNR in beam space. The same plots are shown for time delay matching in Figure 6.29. The distance estimation is less accurate than for the corresponding spherical matching.

The same comparisons are also shown in Figures 6.30 and 6.31, for results obtained with the recursive updating constant α set to 0.5. The BTRs become more stable and display smoother tracks. Also, the distance estimation is more accurate than those made without recursive updating, because the SCM is better conditioned. Using too small value for α can lead to loss in angular variability of the beamformer, thus the ability of tracking fast moving targets is reduced.

[4]See Equation (4.6)

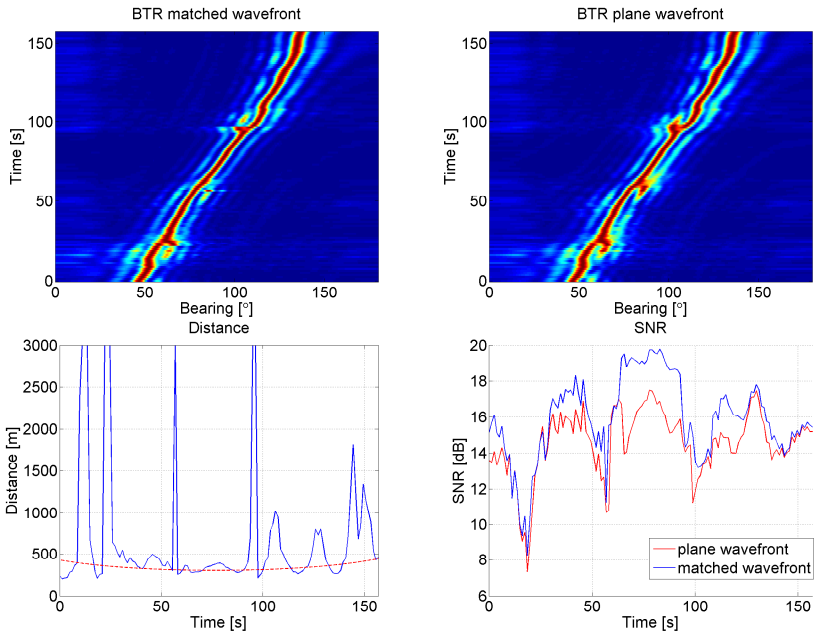

Figure 6.28: BTR estimated with CB using a match to a spherical (top left) and a plane (top right) wavefront. Estimated distance (blue) and real distance (red), bottom left. SNR in beam space for the matched and the plane wavefront, bottom right. No added noise, distance at CPA is 300 m, and no recursive updating of the SCM.

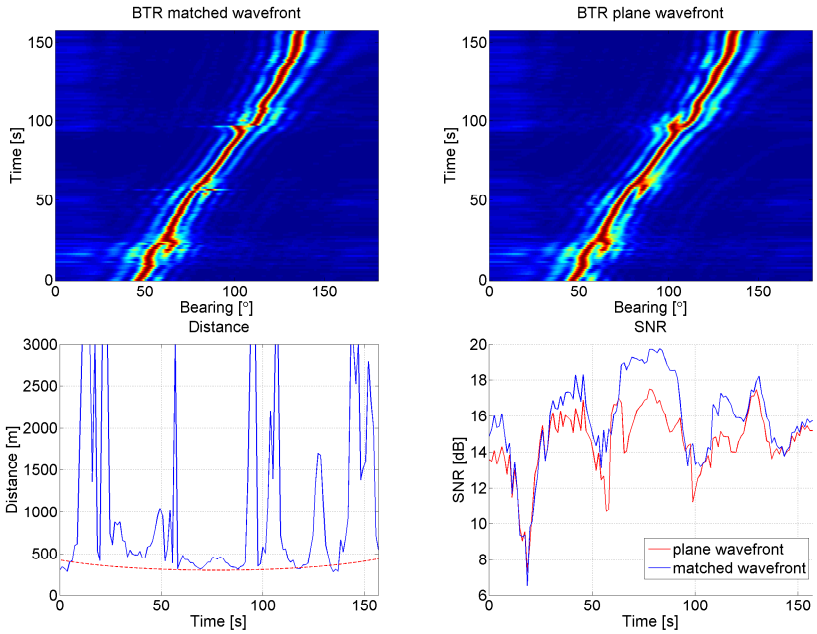

Figure 6.29: BTR estimated with CB using a match by time delay estimates (top left) and to a plane (top right) wavefront. Estimated distance (blue) and real distance (red), bottom left. SNR in beam space for the matched and the plane wavefront, bottom right. No added noise, distance at CPA is 300 m, and no recursive updating of the SCM.

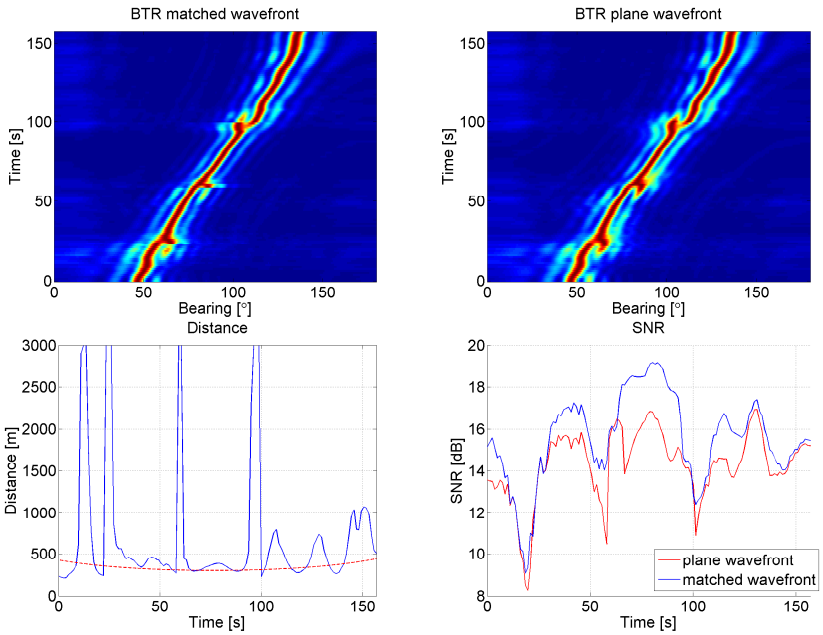

Figure 6.30: BTR estimated with CB using a match to a spherical (top left) and a plane (top right) wavefront. Estimated distance (blue) and real distance (red), bottom left. SNR in beam space for the matched and the plane wavefront, bottom right. No added noise, distance at CPA is 300 m, and the recursive updating constant α is set to 0.5.

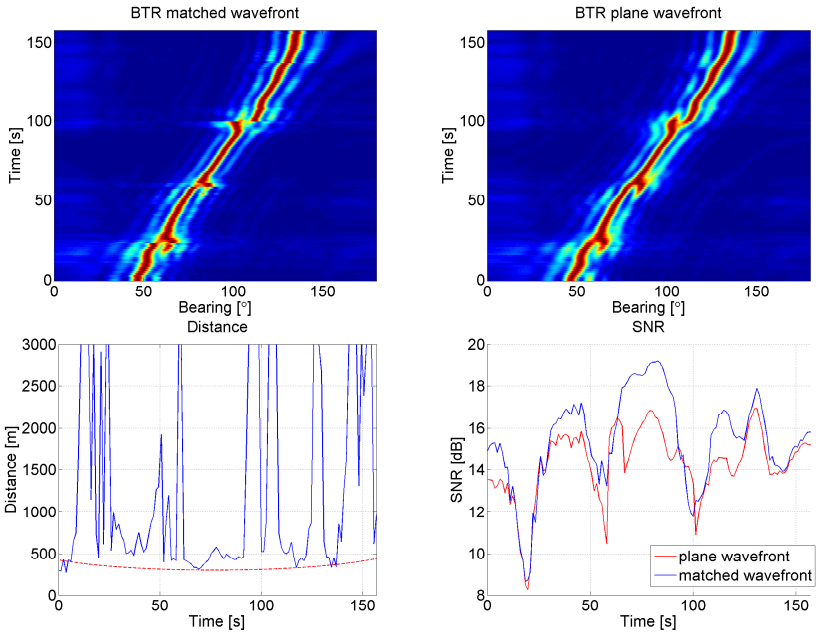

Figure 6.31: BTR estimated with CB using a match by time delay estimates (top left) and to a plane (top right) wavefront. Estimated distance (blue) and real distance (red), bottom left. SNR in beam space for the matched and the plane wavefront, bottom right. No added noise, distance at CPA is 300 m, and the recursive updating constant α is set to 0.5.

6.4.2.2 Beamforming using MUSIC

The number of sources estimation for run 2 is shown in Figure 6.32. The estimation is generally correct (1 source), and becomes more accurate when recursive updating is used, because more data is used in the SCM estimate. Figures 6.33-6.36 display the results of using the MUSIC cost function. Each figure shows a comparison between a matched beamforming method, either spherical or time delay, and plane wave beamforming.

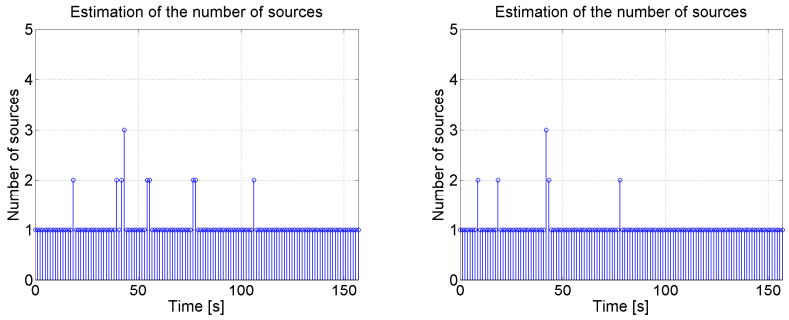

Figure 6.32: Estimation of the number of sources for run 2. No recursive updating of the SCM (left), updating constant set to 0.5 (right).

The results of spherical matching and plane wavefront beamforming obtained without recursive updating of the SCM, are compared in Figure 6.33. The sidelobes are lower for spherical matching, which is evidenced by the presence of more dark regions for the spherical matching BTR plot than in the plane wavefront plot. Also, the bearing track is sharper than when using CB. The SNR in beam space drops down to zero several times because the sidelobes are defined as 3 dB below the maximum of the main lobe, and when the sidelobe levels are higher than 3 dB no SNR value is calculated.

Corresponding plots are shown for time delay matching in Figure 6.34. Again the distance estimation is less accurate than for the corresponding spherical matching.

The same comparisons are shown in Figure 6.35 and 6.36 using a recursive updating constant α set to 0.5. Again the BTRs shows smoother tracks, and the distance estimation is more accurate than when using no recursive updating.

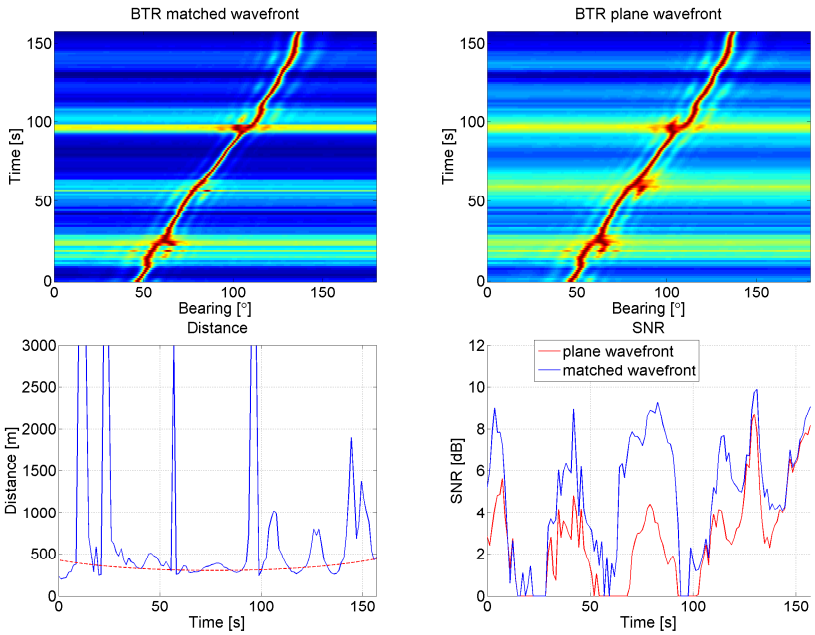

Figure 6.33: BTR estimated with MUSIC using a match to a spherical (top left) and a plane (top right) wavefront. Estimated distance (blue) and real distance (red), bottom left. SNR in beam space for the matched and the plane wavefront, bottom right. No added noise, distance at CPA is 300 m, and no recursive updating of the SCM.

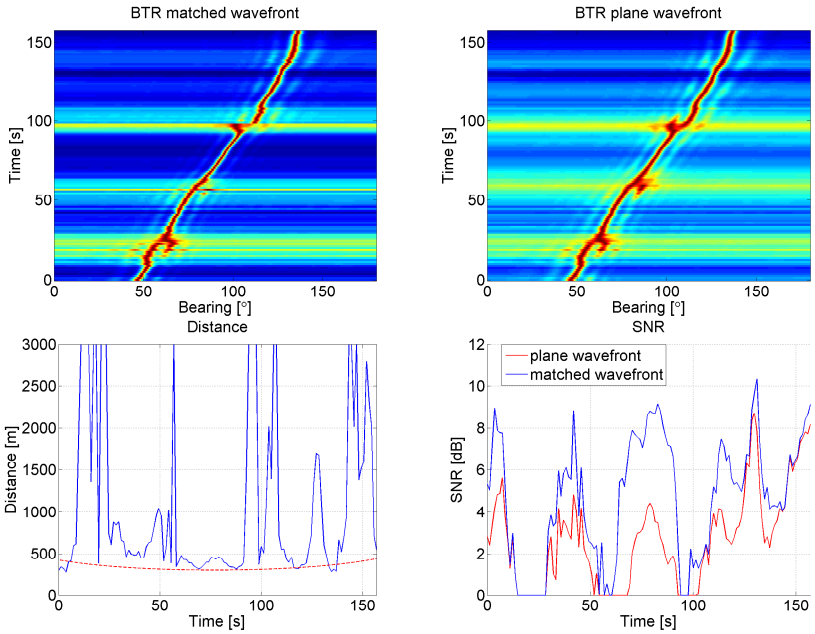

Figure 6.34: BTR estimated with MUSIC using a match by time delay estimates (top left) and to a plane (top right) wavefront. Estimated distance (blue) and real distance (red), bottom left. SNR in beam space for the matched and the plane wavefront, bottom right. No added noise, distance at CPA is 300 m, and no recursive updating of the SCM.

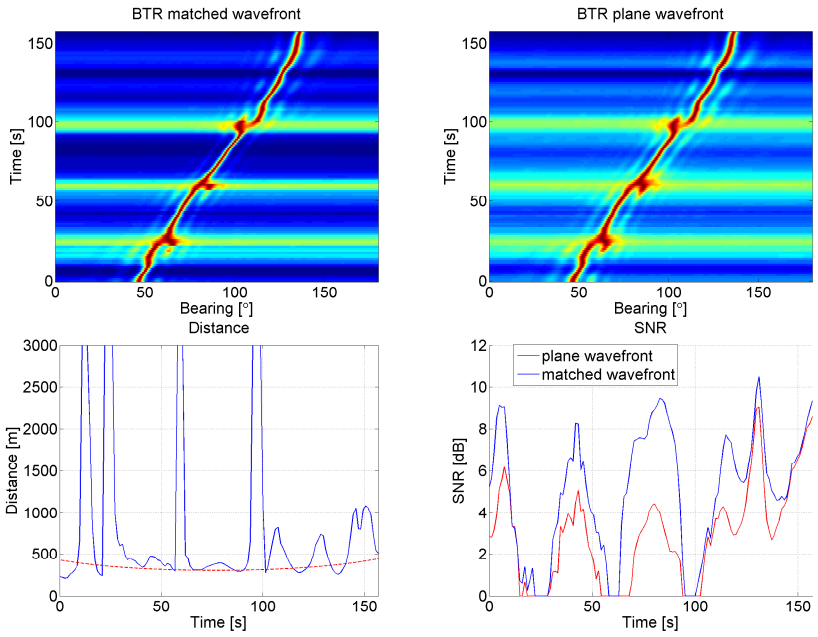

Figure 6.35: BTR estimated with MUSIC using a match to a spherical (top left) and a plane (top right) wavefront. Estimated distance (blue) and real distance (red), bottom left. SNR in beam space for the matched and the plane wavefront, bottom right. No added noise, distance at CPA is 300 m and the recursive updating constant α is set to 0.5.

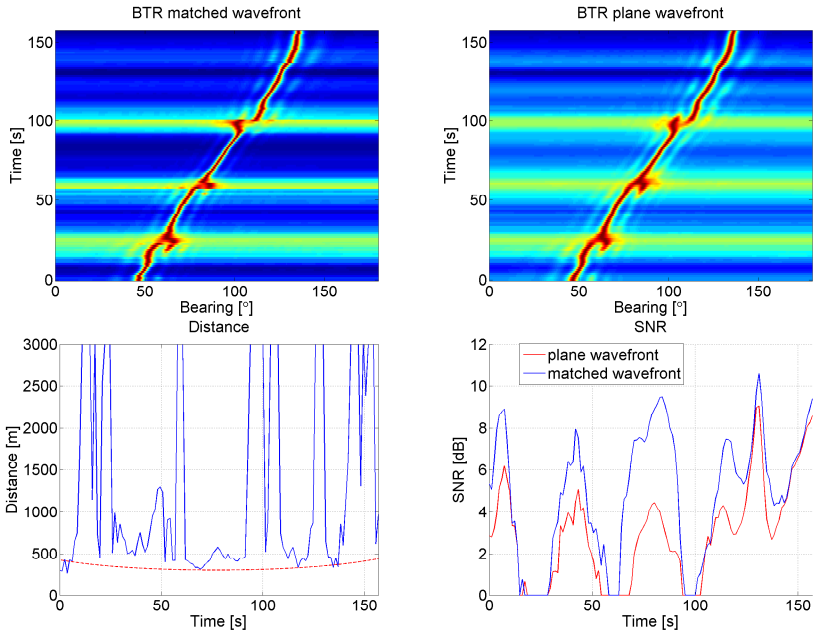

Figure 6.36: BTR estimated with MUSIC using a match by time delay estimates (top left) and to a plane (top right) wavefront. Estimated distance (blue) and real distance (red), bottom left. SNR in beam space for the matched and the plane wavefront, bottom right. No added noise, distance at CPA is 300 m, and the recursive updating constant α is set to 0.5.

6.5 Distance estimation performance: spherical matching compared to a triangulation method

For a comparison of the distance estimation capabilities of the spherical matching, the results are compared to another method referred to as triangulation.

The triangulation method

The triangulation method divides the array into two subarrays. Each subarray yields a bearing estimation, ϕ_1 and ϕ_2. The distance L between the centers of the subarrays is known and by using the laws of sine and cosine, the distance to the target can be estimated. The method is illustrated in Figure 6.37.

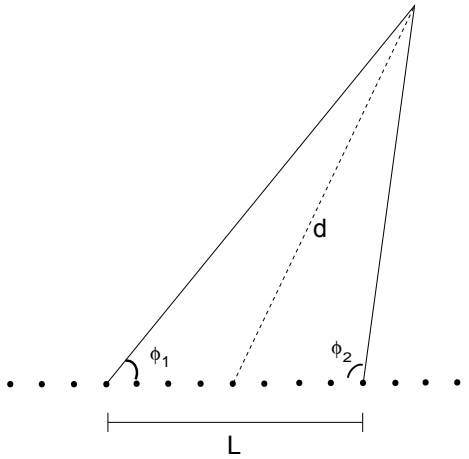

Figure 6.37: Illustration of the triangulation method. The angle ϕ_1 is estimated by the left portion of the array and the angle ϕ_2 is estimated from the right portion of the array; L is the distance between the centers of the arrays; d is the estimated distance to target.

CB is used in the estimations. For the cases when $\phi_1 + \phi_2 > 180°$ the triangulation methods fails (because no triangle is formed), so the estimated distance is assigned a value of zero. Different updating constants have been used in all the estimations.

Figure 6.38 shows the comparisons between the estimated distances obtained from spherical matching and triangulation. For run 1, Figure 6.38(a,c,e), the results of triangulation and spherical matching are similar. For both methods, the smaller the recursive updating constant, the more accurate the results. For run 2, Figure 6.38(b,d,f), the methods yield significantly different results. The triangulation methods demonstrates a tolerance against the high noise level that is present in run 2, whereas the spherical matching experiences severe degradation in the estimation. The reason for this is that the triangulation method is based on bearing estimates, whereas the spherical matching method is based on wavefront estimates, and bearing estimates are more robust in the presence of noise than wavefront estimates.

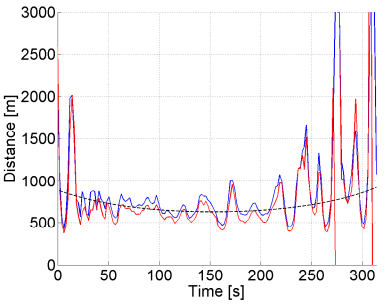

(a) Run 1, no recursive updating.

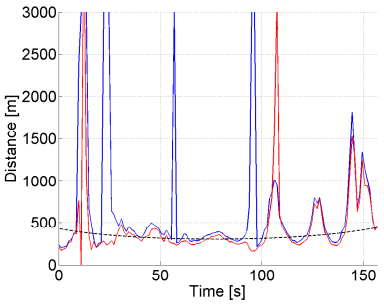

(b) Run 2, no recursive updating.

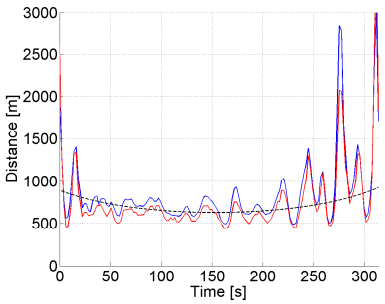

(c) Run 1, α set to 0.5.

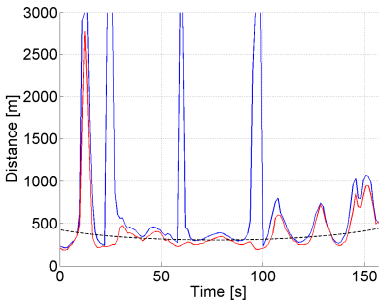

(d) Run 2, α set to 0.5.

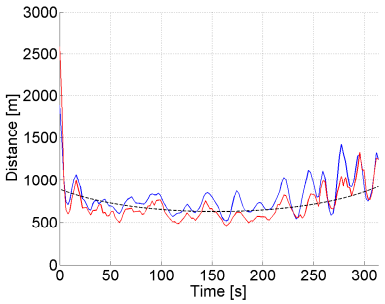

(e) Run 1, α set to 0.25.

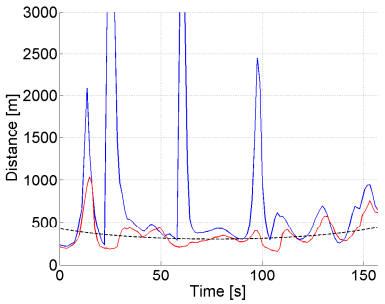

(f) Run 2, α set to 0.25.

Figure 6.38: Distance estimations via spherical matching (blue) and triangulation (red). The real distances are shown in black. Plots (a),(c) and (e) are estimations from run 1 and plots (b), (d) and (f) are estimations from run 2.

7 Conclusions and future work

The aim of this study was to evaluate the advantages of using a beamformer which adjusts the processing depending on the shape of the wavefront (matched beamforming) versus using one which simply assumes the wavefront to be planar (plane-wave beamforming). Data were simulated with Raylab and experimental data was also used to evaluate the methods. Two methods of estimating the shape of the wavefront have been developed: estimating the time delays between sensors, and matching the wavefront to spherical shapes with different radii. Both methods are compared to plane-wave beamforming. Conventional beamforming and MUSIC was used as beamforming algorithms. The results are presented as BTRs, SNRs and distance estimations. Unfortunately there was no GPS data available from the field-test, so a model has been used to approximate the bearing and distance variations.

Findings

In general, it is shown that both matching methods perform better than plane-wave beamforming. However, at low SNRs there is almost no difference between the matched beamforming and the plane wave beamformer, because the noise interfering with the signals makes it difficult to accurately estimate the shape of the wavefront. The simulated data shows that the benefits of using a matched beamformer are greater when the source is closer. Near broadside the difference in performance is 2.5-3 dB when the target is 300 m in front of the array, and 1 dB when the target is 600 m in front of the array. The performance of the matched beamformers degrades and approaches the performance of the plane wave beamformer when the impinging angle of the wave is near endfire of the array. This is because the effective length of the array shrinks for angles near endfire, thus it is increasingly difficult to detect the shape of the wavefront when the array is short. From the experiment in can be concluded that the difference in performance is between 2 dB when the target is 300 m in front of the array and approximately 0.5-1 dB when the array is at 600 m in front of the array.

The distance estimation is difficult due to the small time differences between adjacent sensors. The estimation can be made more accurate with recursive updating of the covariance matrix. The spherical matching method shows more accurate distance estimations compared to the time delay matching results. In addition, the distance estimation for time delay matching shows a biased error. The distance estimations obtained from spherical matching are similar to those of the triangulation method for high SNRs. However, as the SNR decreases the estimations given by spherical matching worsen whereas the estimations given by triangulation are more robust.

Future improvements

For a moving array a form of Synthetic Array Sonar (SAS) could be used, which would increase the effective length of the array and lead to an improvement in the distance estimation. An algorithm that removes incorrect distances could also be used. By using previous values of the distance estimations unrealistic estimates could be removed by setting a threshold that defines a realistic

movement. Another improvement may be to incorporate knowledge about the environment into the processing, but that may lead to additional challenges, due to the potential errors in the model parameters. A hybrid scheme could be used, that utilizes the distance estimation from triangulation and adjusts the steering vectors in the beamformer to the shape corresponding to that distance assuming spherical wavefronts.

Because the current methods are unable to identify multipath, a condition which leads to poor distance estimations due to decreased wavefront curvature, an algorithm that can detect and characterize multipath might lead to improved performance. Furthermore, because knowledge about the sensor positions is critical to the signal processing in sonar systems, using the time delay estimation method for calibration of the sensors positions, may lead to better position estimates and thus better results. The distance estimation algorithm for the time delay method shows a biased error, and thus improvements may be possible.

Bibliography

[1] L. Abrahamsson. Raylab-A ray tracing program in underwater acoustics. Technical Report FOI-R–1047–SE, Sweden Defence Research Agency, 2003.

[2] A. Baggeroer, W.A Kuperman, and H. Schmidt. Matched field processing: Source localization in correlated noise as an optimum parameter estimation problem. *Journal of the Acoustical Society of America*, 83(2):571–587, 1988.

[3] C. Balanis. *Antenna Theory Analysis and Design*. Wiley, 3rd edition, 2005. ISBN 0-471-66782-X.

[4] M. Burdic. *Underwater Acoustic System Analysis*. Prentice-Hall, 1st edition, 1984. ISBN 0-13-936716-0.

[5] W.R Hahn and S.A Tretter. Optimum processing for delay-vector estimation in passive signal arrays. *IEEE Transactions on Information Theory*, 19(5):608–614, 1973.

[6] R.A. Kennedy, T.D. Abhayapala, and D.B. Ward. Broadband nearfield beamforming using a radial beampattern transformation. *IEEE Transactions on signal processing*, 46(8):2147–2156, 1998.

[7] H. Krim and M. Viberg. Two decades of array signal processing research. *IEEE Signal Processing Magazine*, 13(4):67–94, 1996.

[8] H. Lantz, E. Parastates, L. Persson, and Ö. Staaf. Syntetisk aperturanalys av kabelsonardata. FOI-R–0198–SE, Sweden Defence Research Agency, 2001.

[9] M. Lasky, R.D. Doolittle, B.D. Simmons, and S.G. Lemon. Recent progress in towed hydrophone array research. *IEEE Journal Of Oceanic Engineering*, 29(2):374–387, 2004.

[10] R.J Mailloux. *Phased Array Antenna Handbook*. Artech House Publishers, 1st edition, 1993. ISBN 0-89006-502-0.

[11] M. Meister, P. Dieschner, and H. Schmidt. Advanced ranging sonar: Passive ranging with line arrays-sea trial results. *Atlas Elektronik UDT Europe*, 2006.

[12] S. Ravishankar, H.V. Kumaraswamy, and B.D. Satish. Comparative analysis of direction of arrival estimation and beamforming techniques in smart antennas. ObCom: Mobile, Ubiquitous & Pervasive Computing. Vellore Institute of Technology, 2006.

[13] R.O. Schmidt. Multiple emitter location and signal parameter estimation. *IEEE Transactions on antennas and propagation*, 34(3):276–280, 1986.

[14] H.L. Van Trees. *Optimum Array Processing*. Wiley-Interscience, 1st edition, 2002. ISBN 0-471-09390-4.

[15] R.J Urich. *Principles of Underwater Sound*. McGraw-Hill, 3rd edition, 1983. ISBN 0-07-066087-5.

[16] Y.R. Zheng and R.A. Goubran. Robust near-field adaptive beamforming with distance discrimination. *IEEE Transactions on speech and audio processing*, 12(5):478–488, 2004.

A Positions of array elements in the towed array sonar

Array element	Cumulative distance (m)
1	0
2	2.32
3	4.64
4	6.96
5	9.28
6	11.6
7	13.92
8	16.24
9	20.30
10	22.60
11	24.94
12	27.26
13	29.29
14	31.61
15	33.93
16	36.25
17	38.57
18	40.89
19	43.21
20	45.53
21	47.85
22	50.17
23	52.78
24	55.10
25	57.42
26	59.74
27	62.64
28	64.96
29	67.28
30	69.60
31	71.92
32	74.24

B Snell's Law

Figure B.1 illustrates Snell's law for refraction of sound rays.

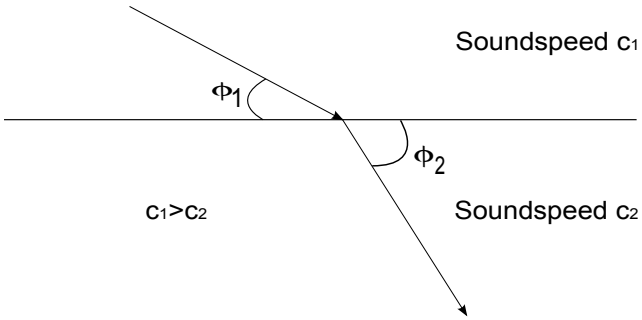

Figure B.1: Diagram of the refraction of sound rays.

With the notation as in Figure B.1 Snell's Law is defined as

$$\frac{\cos(\phi_1)}{\cos(\phi_2)} = \frac{c_1}{c_2}\,. \tag{B.1}$$